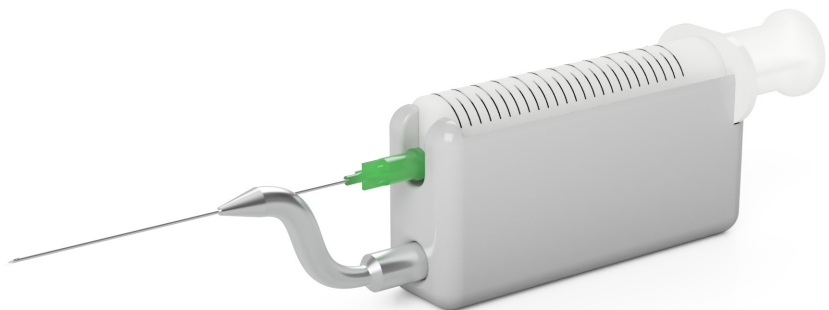


# Ultrasonically Actuated Medical Needle

—  
Non-Linear Effects and Applications

---

Emanuele Perra



# Ultrasonically Actuated Medical Needle

Non-Linear Effects and Applications

**Emanuele Perra**

A doctoral thesis completed for the degree of Doctor of Science (Technology) to be defended, with the permission of the Aalto University School of Science, at a public examination held at the lecture hall 213a of the school (Otakaari 4) on 7 October 2022 at 12 pm.

**Aalto University**  
**School of Science**  
**Department of Neuroscience and Biomedical Engineering**  
**Medical Ultrasonics Laboratory (MEDUSA)**

**Supervising professor**

Professor Heikki J. Nieminen, Aalto University, Finland

**Thesis advisor**

Professor Heikki J. Nieminen, Aalto University, Finland

**Preliminary examiners**

Professor Claude Inserra, Lyon University, France

Professor Adrian Neild, Monash University, Australia

**Opponent**

Professor Michael R. Bailey, University of Washington, WA, United States

Aalto University publication series

**DOCTORAL THESES** 127/2022

© 2022 Emanuele Perra

ISBN 978-952-64-0933-7 (printed)

ISBN 978-952-64-0934-4 (pdf)

ISSN 1799-4934 (printed)

ISSN 1799-4942 (pdf)

<http://urn.fi/URN:ISBN:978-952-64-0934-4>

Unigrafia Oy

Helsinki 2022

Finland



Printed matter  
4041-0619

**Author**

Emanuele Perra

**Name of the doctoral thesis**

Ultrasonically Actuated Medical Needle: Non-Linear Effects and Applications

**Publisher** School of Science**Unit** Department of Neuroscience and Biomedical Engineering**Series** Aalto University publication series DOCTORAL THESES 127/2022**Field of research** Medical Ultrasonics**Manuscript submitted** 10 June 2022**Date of the defence** 7 October 2022**Permission for public defence granted (date)** 17 August 2022**Language** English **Monograph** **Article thesis** **Essay thesis****Abstract**

Medical needles serve a central role in everyday healthcare, exemplified by the 16 billion injections administered globally every year. The needles typically feature a very sharp structure at their tip (lancet), which facilitates the penetration through the skin and tissue to achieve a medical purpose. When used in combination with a syringe, hypodermic needles enable *e.g.* injection of substances into the patient's body, or to extract cells from the target. Despite their extensive use in medicine, the design of medical needles has remained largely unchanged throughout recent decades and limitations related to pain, delivery of entities, precision and spatial localization still remain.

The primary aim of this Thesis was to study how ultrasound can be used to bring new functionalities to a standard medical needle in vision to address major issues still present in some medical applications. The solution consisted in coupling a Langevin transducer ( $f \sim 33$  kHz) to a 21G hypodermic needle (outer diameter = 0.81 mm; length = 80 mm) through an aluminum waveguide to produce flexural standing waves within the needle structure. The experiments focused on exploring the influence of the needle vibration on matter, when the ultrasonically actuated needle was operated in different types of media, such as water, tissue-like phantom gels and *ex vivo* soft tissue. Numerical simulations were also conducted to deepen the understanding of some relevant non-linear ultrasound phenomena involved in the experiments, namely acoustic radiation force, acoustic streaming and cavitation, generated by the oscillating needle.

The results showed that the actuation of a medical needle contributes to generating a force field on the medium surrounding the needle tip, which can be exploited to manipulate soft matter or solid objects. When used to perform ultrasound-enhanced fine-needle aspiration biopsy, the ultrasonic oscillation of the needle allowed to increase the mass of the collected sample by 3–6x in different *ex vivo* bovine tissue types, as compared to when standard fine-needle aspiration biopsies were retrieved. Experimentally and numerically, we were able to demonstrate generation of acoustic streaming emanating outwards from the needle tip, which allowed to translate microparticles inside water, and helped to promote the translation of nanoparticles and liquids inside tissue-like porous structures. Formation of transient cavitation events was also captured with high-speed imaging in water and soft tissue, exhibiting a strong threshold behavior dependent on the total acoustic power employed.

The findings presented in this Thesis advance the field of oscillating medical needles, showing a great potential in various medical applications including biopsy, drug or gene delivery and tissue ablation.

**Keywords** Physics, Non-Linear Ultrasound, Medical Needle, Cavitation**ISBN (printed)** 978-952-64-0933-7**ISBN (pdf)** 978-952-64-0934-4**ISSN (printed)** 1799-4934**ISSN (pdf)** 1799-4942**Location of publisher** Helsinki**Location of printing** Helsinki **Year** 2022**Pages** 127**urn** <http://urn.fi/URN:ISBN:978-952-64-0934-4>



**Tekijä**

Emanuele Perra

**Väitöskirjan nimi**

Ultraääniaktivoitu lääkinällinen neula: epälineaariset vaikutukset ja sovellukset

**Julkaisija** Perustieteiden korkeakoulu**Yksikkö** Neurotieteen ja lääketieteellisen tekniikan laitos**Sarja** Aalto University publication series DOCTORAL THESES 127/2022**Tutkimusala** Lääketieteellinen ultraääni**Käsikirjoituksen pvm** 10.06.2022**Väitöspäivä** 07.10.2022**Väittelyluvan myöntämispäivä** 17.08.2022**Kieli** Englanti **Monografia** **Artikkeliväitöskirja** **Esseeväitöskirja****Tiivistelmä**

Lääkinnällisillä neuiloilla on keskeinen merkitys terveydenhuollossa. Vuosittain annetaan maailmanlaajuisesti esimerkiksi 16 miljardia injektiota. Neulojen kärjessä on yleensä erittäin terävä rakenne (lansetti), joka helpottaa neulan tunkeutumista ihon sisään lääketieteellisen tarkoituksen saavuttamiseksi. Kun injektioneuloja käytetään yhdessä ruiskun kanssa, niitä voidaan käyttää aineiden ruiskuttamiseen potilaan kehoon tai diagnostisesti merkityksellisen materiaalin ottamiseen kohteesta. Vaikka neuvoja käytetään lääketieteessä hyvin laajalti, neulojen muotoilu on pysynyt muuttumattomana vuosikymmenien ajan, ja kipuun, kokonaisuusien hallintaan, tarkkuuteen ja spatiaaliseen paikantamiseen liittyvät rajoitukset ovat edelleen olemassa.

Tämän opinnäytetyön ensisijaisena tavoitteena oli tutkia, miten ultraääntä voidaan hyödyntää tuomaan uutta toiminnallisuutta tavalliseen lääketieteelliseen neulaan ja kyetään vähentämään eräissä lääketieteellisissä sovelluksissa esiintyviä merkittäviä ongelmia. Ratkaisu koostuu Langevin-muuntimen ( $f \sim 33$  kHz) kytkemisestä 21G-injektioneulaan (ulkohalkaisija = 0.81 mm; pituus = 80 mm) alumiinisen aalto-ohjaimen kautta. Näin neulan rakenteeseen aikaansaadaan neulan taivutuksen mahdollistavat seisovat aallot. Kokeissa keskityttiin tutkimaan neulan flexuraalisen värähtelyn vaikutusta aineeseen, kun ultraäänikäyttöistä neulaa käytettiin erityyppisissä väliaineissa, kuten vedessä, kudosisäilytysväliaineissa ja *ex vivo* pehmytkudoksessa. Numeerisia simulaatioita hyödynnettiin syventämään ymmärrystä eräistä kokeisiin liittyvistä värähtelevän neulan luomista epälineaarisen ultraäänien ilmiöistä kuten akustisesta säteilyvoimasta, akustisesta virtauksesta ja kavitaatiosta.

Tulokset osoittivat, että lääkinällinen neula tuottaa neulan kärkeä ympäröivään väliaineeseen voimakentän, jota voidaan hyödyntää pehmeän aineen tai kiinteiden esineiden käsittelyssä. Kun ultraäänitehostettua ohutneulanäytteenottoa käytettiin biopsioiden ottamiseen, neulan ultraäänivärähtely mahdollisti kerätyn näytteen massan kasvamisen 3-6-kertaiseksi erilaisissa naudan kudostyypeissä verrattuna tavanomaisiin ohutneulanäytteenottoihin. Kokeellisesti ja numeerisesti pystyimme osoittamaan neulan kärjestä ulospäin lähtevän akustisen virtauksen syntymisen, joka mahdollisti mikrohiukkasten kääntämisen veden sisällä ja auttoi edistämään nanohiukkasten ja nesteiden kääntämistä kudoksen kaltaisten huokosten rakenteiden sisällä. Myös lyhytaikaisten kavitaatiotahtumien muodostumista kuvattiin nopealla kuvantamisella sekä vedessä että pehmytkudoksessa. Niissä ilmeni voimakas kynnyskäyttäytyminen, joka riippui käytetystä akustisesta kokonaistehosta.

Tässä väitöskirjassa esitetyt havainnot edistävät värähtelevien lääketieteellisten neulojen alaa, ja

**Avainsanat** Fysiikka, epälineaarinen ultraääni, lääketieteellinen neula, kavitaatio**ISBN (painettu)** 978-952-64-0933-7**ISBN (pdf)** 978-952-64-0934-4**ISSN (painettu)** 1799-4934**ISSN (pdf)** 1799-4942**Julkaisupaikka** Helsinki**Painopaikka** Helsinki**Vuosi** 2022**Sivumäärä** 127**urn** <http://urn.fi/URN:ISBN:978-952-64-0934-4>



**Författare**

Emanuele Perra

**Doktorsavhandlingens titel**

Ultraljudaktiverad nål för medicinskt bruk: icke-linjära effekter och applikationer

**Utgivare** Högskolan för teknikvetenskaper**Enhet** Institutionen för neurovetenskap och biomedicinsk teknik**Seriens namn** Aalto University publication series DOCTORAL THESES 127/2022**Forskningsområde** Medicinsk ultraljud**Inlämningsdatum för manuskript** 10.06.2022**Datum för disputation** 07.10.2022**Beviljande av disputationstillstånd (datum)** 17.08.2022**Språk** Engelska **Monografi** **Artikelavhandling** **Essäavhandling****Sammandrag**

Medicinska nålar har en central roll i sjukvården, vilket framgår av de 16 miljarder injektioner som ges globalt årligen. De har vanligtvis en mycket skarp struktur i spetsen (lansett) som gör det lättare för nålen att trängas in i huden för att uppnå ett medicinskt syfte. I kombination med en spruta kan hypodermiska nålar användas för att injicera ämnen i patientens kropp eller för att erhålla diagnostiskt relevant material från målet. Trots den mycket omfattande användningen inom medicinen har utformningen av medicinska nålar förblivit oförändrad under årtiondena och begränsningar i fråga om smärta, leverans av enheter, precision och rumslig lokalisering kvarstår fortfarande.

Det primära syftet med denna avhandling var att studera hur ultraljud kan användas för att ge nya funktioner till en medicinsk standardnål för att minska de stora problem som fortfarande kvarstår i vissa medicinska tillämpningar. Lösningen bestod i att koppla en Langevin-transducer ( $f \sim 33$  kHz) till en 21G hypodermisk nål (ytterdiameter = 0.81 mm; längd = 80 mm) genom en aluminiumvågledning, så att böjbara stående vågor skulle aktiveras i nålens struktur. Experimenten inriktades på att utforska hur nålens vibrationer påverkar materia när den ultraljudsstyrda nålen användes i olika typer av medier, t.ex. vatten, vävnadsliknande fantomgeler och *ex vivo* mjuk vävnad. Även numeriska simuleringar genomfördes för att uppnå fördjupad förståelse av vissa relevanta icke-linjära ultraljudsfenomen vilka var inblandade i experimenten, nämligen akustisk strålningskraft, akustisk strömning och kavitation, som genereras av den vibrerande nålen.

Resultaten visade att aktiveringen av en medicinsk nål bidrar till att generera ett kraftfält i det medium som omger nålspetsen, vilket kan utnyttjas för att manipulera mjuka material eller fasta föremål. När nålens ultraljudsvibrationer användes för att utföra ultraljudsförstärkta finnålsaspirationsbiopsier, kunde nålens ultraljudsvibrationer öka massan av det insamlade provet med 3-6× i olika vävnadstyper av nötkreatur, jämfört med vanliga finnålsaspirationsbiopsier. Experimentellt och numeriskt kunde vi visa att det genererades en akustisk strömning utåt från nålspetsen, vilket gjorde det möjligt att översätta mikropartiklar i vatten och bidrog till att främja översättningen av nanopartiklar och vätskor i vävnadsliknande porösa strukturer. Bildandet av övergående kavitationshändelser fångades också med höghastighetsbilder i vatten och mjuk vävnad och uppvisade ett starkt tröskelbeteende som var beroende av den totala akustiska effekten som användes.

De resultat som presenteras i den här avhandlingen innebär ett framsteg inom området vibrerande

**Nyckelord** Fysik, icke-lineär ultraljud, nål för medicinskt bruk, kavitation**ISBN (tryckt)** 978-952-64-0933-7**ISBN (pdf)** 978-952-64-0934-4**ISSN (tryckt)** 1799-4934**ISSN (pdf)** 1799-4942**Utgivningsort** Helsingfors**Tryckort** Helsingfors**År** 2022**Sidantal** 127**urn** <http://urn.fi/URN:ISBN:978-952-64-0934-4>



# Preface

The work presented in this Thesis has been conducted between February 2018 and October 2022 in the Medical Ultrasonics (MEDUSA) research group at the Department of Neuroscience and Biomedical Engineering, Aalto University, Finland. The research grants awarded by Academy of Finland and Foundation for Aalto University Science and Technology are gratefully acknowledged.

First and foremost I would like to thank my supervisor Prof. Heikki J. Nieminen for his invaluable guidance and support - without him, I would have not been able to achieve such an ambitious goal. I am also grateful to pre-examiners Prof. Claude Inserra and Prof. Adrian Neild for their thorough review and constructive criticism, and I thank Prof. Michael R. Bailey for agreeing to act as opponent in the defense.

I thank all former and present members of the MEDUSA group for their support and for creating a friendly work environment, even during the lockdown. I would like to thank all my co-authors, especially Kenneth P.H. Pritzker, MD, and Dr. Gonçalo Barreto, for their knowledge and expertise. Special thanks go to Dr. Nick Hayward for linguistic review of the manuscripts, and for providing emotional support and mentorship throughout the years.

I would also like to extend my sincere thanks to all my friends whose love and support accompanied me during this journey. Thank you all for always being there. I cherish fondly the good times and the sweet memories that we shared together.

Lastly, I am deeply thankful to my parents, Daniele and Lucia, and to my brother, Renato, for their endless love, and for being my major source of strength, motivation and inspiration.

Espoo, September 7, 2022,

Emanuele Perra



# Contents

<b>Preface</b>	<b>1</b>
<b>Contents</b>	<b>3</b>
<b>List of Publications</b>	<b>5</b>
<b>Author's Contribution</b>	<b>7</b>
<b>List of Figures</b>	<b>9</b>
<b>Abbreviations</b>	<b>13</b>
<b>Symbols</b>	<b>15</b>
<b>1. Introduction</b>	<b>19</b>
1.1 Aims of the Study . . . . .	21
<b>2. Background</b>	<b>23</b>
2.1 Linear Acoustics . . . . .	23
2.1.1 The linear acoustic wave equation . . . . .	24
2.1.2 Reflection and transmission of sound . . . . .	27
2.1.3 Attenuation of sound . . . . .	31
2.2 Non-Linear Ultrasound . . . . .	33
2.2.1 Acoustic radiation force . . . . .	34
2.2.2 Acoustic streaming . . . . .	35
2.2.3 Cavitation . . . . .	36
2.2.4 Shockwaves . . . . .	38
<b>3. Methods</b>	<b>39</b>
3.1 Experimental Arrangements . . . . .	39
3.1.1 Ultrasonic device . . . . .	39
3.1.2 Electronics . . . . .	40

3.1.3	Optics . . . . .	40
3.1.4	Software . . . . .	41
3.1.5	Samples . . . . .	42
3.2	Numerical Simulations . . . . .	43
3.2.1	Geometry and materials . . . . .	43
3.2.2	Needle motion . . . . .	43
3.2.3	Acoustic field . . . . .	44
3.2.4	Acoustic streaming . . . . .	44
3.2.5	Cavitation . . . . .	45
<b>4.</b>	<b>Summary of publications</b>	<b>47</b>
4.1	Publication I . . . . .	47
4.2	Publication II . . . . .	49
4.3	Publication III . . . . .	51
<b>5.</b>	<b>Discussion</b>	<b>53</b>
<b>6.</b>	<b>Conclusion</b>	<b>57</b>
	<b>References</b>	<b>59</b>
	<b>Publications</b>	<b>69</b>

# List of Publications

This Thesis consists of an overview of the following publications, which are referred to in the text by their Roman numerals.

**I** Emanuele Perra, Eetu Lampsjärvi, Gonçalo Barreto, Muhammad Arif, Tuomas Puranen, Edward Hægström, Kenneth P. H. Pritzker and Heikki J. Nieminen. Ultrasonic Actuation of a Fine-Needle Improves Biopsy Yield. *Scientific Reports*, 11(1), 8234, April 2021.

**II** Emanuele Perra, Nick Hayward, Kenneth P. H. Pritzker and Heikki J. Nieminen. An Ultrasonically Actuated Needle Promotes the Transport of Nanoparticles and Fluids. *The Journal of Acoustical Society of America*, 152(1), 251-265, July 2022.

**III** Emanuele Perra, Nick Hayward, Kenneth P. H. Pritzker and Heikki J. Nieminen. An Ultrasonically Actuated Fine-Needle Creates Cavitation in Bovine Liver. *The Journal of Acoustical Society of America*, 151(6), 3690-3702, June 2022.



# Author's Contribution

## **Publication I: “Ultrasonic Actuation of a Fine-Needle Improves Biopsy Yield”**

E.P., E.L., G.B., M.A., T.P., E.H., K.P.H.P. and H.J.N. contributed to the design of the study, writing or reviewing the manuscript and have approved the final version of the manuscript. E.P. produced all data and conducted all data analysis, except K.P.H.P. and E.P. also analyzed the histology images. E.P. was responsible for the histology process. H.J.N, E.L., K.P.H.P. and E.H. designed the prototype.

## **Publication II: “An Ultrasonically Actuated Needle Promotes the Transport of Nanoparticles and Fluids”**

All authors contributed to the design of the study, writing or reviewing the manuscript and have approved the final version of the manuscript. E.P. produced all data, conducted the data analysis and wrote the first version of the manuscript.

## **Publication III: “An Ultrasonically Actuated Fine-Needle Creates Cavitation in Bovine Liver”**

All authors contributed to the design of the study, writing or reviewing the manuscript and have approved the final version of the manuscript. E.P. produced all data, conducted the data analysis and wrote the first version of the manuscript.



# List of Figures

2.1	Elemental volume of fluid with size $dV = dx dy dz$ . . . . .	24
2.2	Schematic representing the deformation of an elemental volume of fluid along the $x$ direction. . . . .	25
2.3	Reflection and transmission of a plane wave at the interface between two media. . . . .	28
2.4	Reflection and transmission of an oblique incident plane wave at the interface between two media. . . . .	29
2.5	Schematics describing a non-inertial and inertial cavitation event. . . . .	37
3.1	Schematic depicting the custom-made ultrasonic device employed in the experiments. . . . .	40

4.1 Example of NLU phenomena generated with the ultrasonically actuated needle. **(a)** HS frame representing a cavitation event. The needle is embedded in deionized water, and the areas enclosed within the white lines represent cavitating bubbles. **(b)** The needle is operated in air, while a small water droplet is placed at its tip. During sonication, the water droplet is broken up into several micro-droplets, whose size was inversely proportional to the driving frequency. **(c)** When the needle is operated in ballistic gelatin, cavitation activity and streaming was observed. Fluorescence nanoparticle delivered through the needle enabled visualization of the spatial distribution of the nanoparticles induced by US. **(d)** Velocity map of the acoustic streaming generated in water by the ultrasonically actuated medical needle. It can be noticed how the streaming emanates from both sides of the needle tip with directionality. These results show that the ultrasonic energy is highly concentrated at the needle tip, manifesting as formation of different NLU phenomena depending on the medium, where the needle is actuated. These NLU phenomena could potentially bring new functionalities to a standard medical needle. . . . . 48

4.2 Mass of the extracted sample obtained from different *ex vivo* bovine tissues by using the FNABs and USEFNABs. When US energy was employed to perform the biopsies, the yield mass was increased up to 3–6×, as compared to when FNABs were carried out. . . . . 49

4.3 **(a)** Numerical simulation of an ultrasonically assisted injection in liver tissue. **(b)** When the needle is actuated at the relatively low TAP of 20 mW, the volume covered by nanoparticles is increased by three times, as compared to a standard needle injection. These results indicate that the ultrasonic action of the needle could increase the uptake of fluid caused by the enhanced delivery localized near the needle tip, which could be useful for delivering substances into tissues with compromised perfusion. . . . 50

- 4.4 Representation of some relevant acoustic variables evaluated on a cross-sectional plane located at  $z = -0.5$  mm from the needle tip. **(a)** Shows the absolute pressure field radiated from the needle boundary, while **(b)** represents the Gor'kov potential, which denotes the level of attraction of the nanoparticles within the acoustic field and **(c)** represents the ARF acting on the liquid, which gives rise to **(d)** the streaming patterns. In Publication II it was demonstrated that the ARF acting on the liquid is two orders of magnitude greater compared to the force acting on the nanoparticles alone, revealing that the latter brings a negligible contribution to the acceleration of nanoparticles. The results also show that the streaming is highly localized at the sharp-edges of the needle geometry **(d)**, resembling the so called sharp-edge streaming reported in literature. . . . . 51
- 4.5 **(a)** Exemplary HS video frames showing cavitation events taking place at the needle tip at 3 different TAP levels. **(b)** The probability maps, which show the probability of each pixel belonging to an optical projection of a cavitation bubble, demonstrate that no cavitation activity is recorded at 0.2 W, while it is more frequent at higher TAP levels. These results show how cavitation can be generated on-demand and in a localized manner near the needle tip. . . 52



# Abbreviations

**ARF** Acoustic Radiation Force

**CAD** Computer-Aided Design

**FNAB** Fine-Needle Aspiration Biopsy

**HIFU** High-Intensity Focused Ultrasound

**HIU** High-Intensity Ultrasound

**HS** High-speed

**NLU** Non-linear Ultrasound

**OPT** Optical Projection Tomography

**PIV** Particle Image Velocimetry

**TAP** Total Acoustic Power

**US** Ultrasound

**USeFNAB** Ultrasound-Enhanced Fine-Needle Aspiration Biopsy

**WHO** World Health Organization



# Symbols

$a$  Acceleration

$A$  Cross-sectional area

$\mathcal{B}$  Adiabatic bulk modulus

$c$  Speed of sound

$d_r$  Drag coefficient

$E_{ac}$  Acoustic energy

$F_m$  Volume force

$F_{rad}$  Acoustic radiation force

$I$  Acoustic intensity

$\ell$  Discontinuity distance

$m$  Mass

$n$  Number of coil turns

$M$  Mach number

$k$  Wave number

$\vec{k}$  Wave vector

$P$  Instantaneous pressure at location  $(x, y, z)$

$P_\infty$  Ambient liquid pressure

$P_0$  Equilibrium pressure

$P_B$  Blake pressure

$P_{Lan}$  Langevin radiation pressure

Symbols

$P_w, p$  Acoustic pressure

$\vec{r}$  Position vector

$R$  Reflection coefficient; bubble radius; resistance

$R_B$  Blake critical radius

$S$  Surface area; infinitesimal stress tensor

$T$  Transmission coefficient

$t$  Time variable

$T$  Cauchy stress tensor

$u$  Displacement

$v$  Particle velocity

$V$  Volume

$z$  Acoustic impedance

$Z$  Electrical impedance

$\alpha$  Spatial attenuation coefficient

$\alpha_s$  Absorption coefficient due to viscous losses

$\beta$  Coefficient of non-linearity; angle of rotation

$\gamma$  Ratio of heat capacities

$\Gamma$  Gol'dberg number

$\delta$  Sound diffusivity

$\eta$  Coefficient of shear viscosity

$\eta_B$  Coefficient of bulk viscosity

$\theta$  Angle of incidence

$\lambda$  Wavelength

$\xi$  Particle displacement; primary bevel angle

$\Pi_a$  Total absorbed power

$\Pi_s$  Total scattered power

$\rho_0$	Equilibrium density
$\rho_w, \rho_f$	Density fluctuation
$\sigma$	Surface tension
$\tau_s$	Relaxation time
$\phi$	Secondary bevel angle
$\omega$	Angular frequency



# 1. Introduction

The earliest records of the use of medical needles are found in the Greek and Roman literature, where instruments called *puoulkos* (πυουλόκος), serving a similar purpose to that of hypodermic needles, were mentioned to be used in human surgery [1]. Unlike modern hypodermic needles, these instruments were not designed to penetrate the skin, and their functions were limited to draining pus or injecting substances into the body through natural orifices. First documented experiments with hypodermic needles only date back to the 17th century, when goose quills, acting as needles, were used in combination with animal bladders to perform intravenous injections in dogs [1]. However, the first successful injection was carried out on a human subject in 1844, at the Meath Hospital in Dublin [2]. The needle employed in this procedure was made of a hollow steel tube, featuring a bevelled point to one end, and a hub (an access for the syringe or other components) to the other. Ever since, the basic design of the needle has remained largely unchanged, apart from few improvements regarding their safety introduced over the years.

Hypodermic needles currently represent an indispensable medical tool, and they are widely used in everyday health care, according to the estimation of 16 billion injections administered every year, as provided by the World Health Organization (WHO) [3]. They are essentially used for cutting and piercing purposes, thanks to the presence of at least two converging cutting edges and a sharp tip — this structure is usually referred to as the *lancet* [4]. Since they enable minimally invasive percutaneous procedures, they are mainly used to deliver substances into a target inside the body (*e.g.*, drug delivery, anesthesia) or to remove samples of tissue for diagnostic purposes. However, despite their essential role in medicine, previous literature suggests that some needle functions still present limitations with regard to pain [5, 6, 7, 8], spatial localization [9] and for

needle biopsies, adequacy with regard to quality and quantity of tissue yield [10, 11, 12, 13].

Ultrasound (US), which is sound with frequencies greater than 20 kHz, has been recently used as a way to actuate medical needles, because it provides an energy component that can enhance the functions of medical needles. For example, a recent study demonstrates that ultrasonic actuation of hypodermic needles can be used to induce tissue movement to improve the localization of the needle under Doppler US [14, 15, 16] or to facilitate the penetration of the needle into the skin [17, 18]. Actuation of micro-needles has also revealed to be useful in *in vitro* fertilization applications [19, 20], as it can assist the penetration of smaller targets, such as oocytes [21, 22, 23, 24], mouse embryos [25, 26] and fish eggs [27, 28]. Similarly, non-linear ultrasound (NLU) has been applied to tubular structures, *e.g.* to achieve ejection of microdroplets from a tapered glass capillary resonant actuator [29], or to induce ultrasonic standing waves in circular glass capillaries for acoustic trapping of microparticles [30, 31, 32]. Despite limited literature exists on the topic, the use of US in the context of medical needles has drawn the interest of researchers thanks to the enormous potential that ultrasonics have brought to the medical field. Ultrasonic energy has been in fact used to functionalize medical instruments such as surgical knives, to achieve separation of soft tissue by means of protein denaturation [33, 34, 35], or functionalize tools used in dentistry applications, in order to provide a good means of facilitating dental scaling or application of local anesthetics [36, 37].

Generation of highly concentrated ultrasonic beams can also be used to induce the formation of NLU phenomena in a medium, which have been exploited in various therapeutic applications, such as in tumor ablation [38, 39, 40] blood brain barrier opening [41, 42, 43], targeted drug delivery [44, 45, 46, 47] and more [48, 49, 50, 51]. Such phenomena include localized control of cavitation, translation of micro/nanoparticles, micro-bubbles and fluids inside tissues or bodily cavities and generation of microdroplets. However, to date, no research seems to have been conducted to demonstrate the potential of ultrasonically actuated needles in generating these NLU phenomena.

While not yet studied, the use of ultrasonically oscillating needles in medicine could contribute to various medical applications. Potential application areas include drug or gene delivery into cells [52], permeation of tissue allowing entry of therapeutics (*e.g.*, as ultrasonically mediated

blood brain barrier opening) [53, 54], minimally invasive surgical interventions by homogenizing tissues [55], fractionation of calculi [56] and delivery of therapeutic agents such as drugs or distribution of antiseptics in pulmonary conditions [57].

Until now, the possibilities of the widely accepted and used medical needle have been under-explored as a way to mediate and facilitate ultrasonic actuation at a target site. The conventional medical needle could be considered as a minimally invasive and cost-effective enabler of many of precision medicine applications, if its current functions extended beyond its current roles.

## 1.1 Aims of the Study

The general aim presented in this Thesis is to advance the knowledge of ultrasonically oscillating needles, which could potentially bring benefit to a variety of medical applications. An ultrasonic device operating at the frequency of  $\sim 33$  kHz, capable of enabling mechanical flexural standing waves in a conventional hypodermic needle, was investigated, and its effects on different kinds of media were studied.

The specific aims of the study were to:

1. Characterize, quantitatively and qualitatively, the NLU phenomena, *e.g.*, cavitation, acoustic streaming, acoustic radiation force (ARF) and atomization, induced by the ultrasonically oscillating needle tip in different media, such as in water, tissue-mimicking materials and *ex vivo* soft tissue;
2. Provide insight of the physics involved through numerical modeling and experiments;
3. Explore and discuss the use of the studied NLU phenomena in the context of selected medical applications, such as USeFNAB, enhanced drug delivery, tissue ablation and more.



## 2. Background

This section introduces the basic theory of linear and non-linear ultrasonics.

### 2.1 Linear Acoustics

US is typically a pressure wave propagating in a medium with spatial oscillations of the medium at a frequency greater than 20 kHz. The pressure perturbations within the medium cause the particles to displace around their equilibrium position. Depending on the mechanical and material properties of the medium, the wave can propagate in different ways. A particle is here defined in terms of continuum mechanics: it represents an idealized point of a medium, which may contain several molecules, and its dimension is negligible compared to the spatial variation of the acoustic variables within the medium. In fluids, sound waves only propagate as longitudinal waves, where the particle motion is in the same direction of the wave propagation. These types of waves are also called *compression waves*, because they usually consist of a compression phase, characterized by higher pressure due to increased local particle density, followed by a *rarefaction phase*, where the pressure is lower due the particles being farther from each other. In solids, the particles are often strongly bonded to each other, permitting also other modes of propagation such as shear waves, where the particle motion is perpendicular to the direction of the wave propagation, surface waves, which propagate on the material surface, and plate waves, which take place in structures that are usually a few wavelengths thick [58, 36]. When the amplitude of the particle displacement is low enough, the US wave propagates linearly within the medium, where the relationship between the pressure, velocity and density fluctuation are assumed to be linear. Since in the linear regime the propagation

of the ultrasonic wave is not expected to alter significantly the material properties, linear US for instance, represents the simplest nondestructive technique for evaluating material degradation, as a way to detect large defects and cracks within a medium [59]. In these applications, the input signal has small amplitudes, and the output signal, which arises from the scattering, reflection or transmission of the ultrasonic wave at the boundaries of acoustic discontinuities, is assumed to be of the same frequency of the input signal.

### 2.1.1 The linear acoustic wave equation

The propagation of acoustic waves can be described mathematically, and the solution of its constitutive equations can be used to predict the behaviour of ultrasonic waves in the medium they are travelling in. Since in most applications the linear approximation to the wave equation is a good model, in this section, the basic derivation of the linear acoustic wave equation will be covered.

Consider a spatially fixed elemental volume with width, depth and height defined by  $dx$ ,  $dy$  and  $dz$ , respectively, mass  $dm$ , density  $\rho$  and volume  $dV = dx dy dz$ . The net force acting on the elemental volume along the  $x$ -axis direction can be expressed as:

$$df_x = \left[ P - \left( P + \frac{\partial P}{\partial x} dx \right) \right] dy dz = -\frac{\partial P}{\partial x} dV, \quad (2.1)$$

where  $P = P_0 + P_w$  is the instantaneous pressure at  $(x, y, z)$ , defined as the sum of the ambient pressure  $P_0$  and the pressure fluctuation  $P_w$ . Equation

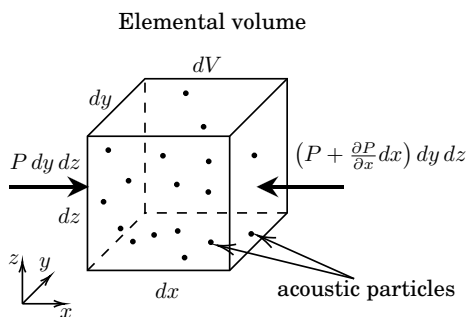


**Figure 2.1.** Elemental volume of fluid with size  $dV = dx dy dz$ .

(2.1) states that the net force experienced by the element is proportional to the negative gradient of the pressure along the positive direction of the  $x$  axis. This means that the acoustic particles will tend to move where the total pressure is the lowest. By applying the second Newton's law,

the equilibrium of forces exerted on the element along the  $x$  axis can be written as:

$$df_x = -dV \frac{\partial P}{\partial x} = dm a_x = \rho dV \frac{\partial^2 \xi_x}{\partial t^2}. \quad (2.2)$$

After integrating (2.2) in respect to the volume one obtains:

$$\rho \frac{\partial^2 \xi_x}{\partial t^2} = -\frac{\partial P}{\partial x}, \quad (2.3)$$

where  $\rho = \rho_0 + \rho_w$  is the instantaneous density at  $(x, y, z)$ , defined as the sum of the equilibrium density  $\rho_0$  and density fluctuation  $\rho_w$ , and  $\xi_x$  is the  $x$  component of the particle displacement, denoting the  $x$  displacement of a particle from its equilibrium location  $x_0$ . The relationship between  $\xi_x$

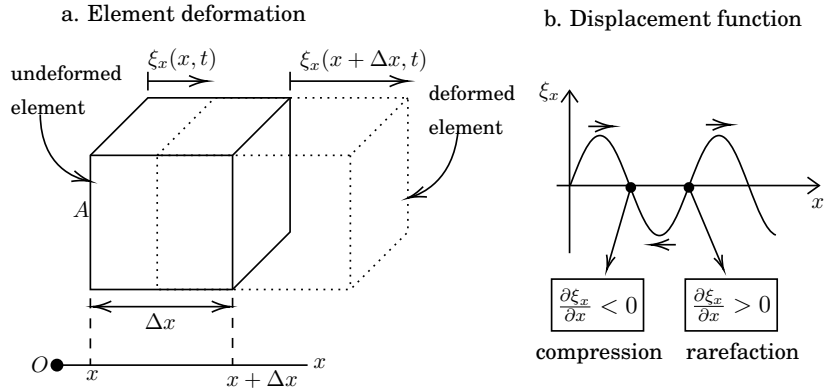


**Figure 2.2.** Schematic representing the deformation of an elemental volume of fluid along the  $x$  direction.

and  $\rho_w$  can be obtained by first considering an element with cross-sectional area  $A$ , initial volume  $V = \Delta x A$ , density  $\rho_0$  and mass  $m$  (Figure 2.2a). Assuming a deformation  $\xi_x$  along the  $x$  axis, the volume of the deformed element will be  $V + \Delta V = (\Delta x + \xi_x(x + \Delta x, t) - \xi_x(x, t)) A$ . Since the mass  $m$  remains constant, the product of the density and the volume also remains constant. As a results, one can write:

$$\rho = \rho_0 + \rho_w = \rho_0 \frac{V}{V + \Delta V} = \rho_0 \frac{\Delta x}{\Delta x + \xi_x(x + \Delta x, t) - \xi_x(x, t)}, \quad (2.4)$$

where  $\rho$  is the density of the deformed element. By rearranging (2.4), one can obtain the following relationship:

$$\rho_w = -\rho_0 \frac{\xi_x(x + \Delta x, t) - \xi_x(x, t)}{\Delta x + \xi_x(x + \Delta x, t) - \xi_x(x, t)}. \quad (2.5)$$

By taking the limit of (2.5) for  $\Delta x \rightarrow 0$ , and assuming small deformations  $\xi_x(x, t)$ , one has:

$$\rho_w = \lim_{\Delta x \rightarrow 0} -\rho_0 \frac{\xi_x(x + \Delta x, t) - \xi_x(x, t)}{\Delta x + \xi_x(x + \Delta x, t) - \xi_x(x, t)} = -\rho_0 \frac{\partial \xi_x(x, t)}{\partial x}. \quad (2.6)$$

According to (2.6) the density fluctuation is proportional to the negative gradient of the displacement function (Figure 2.2b), suggesting that the density tends to build-up when the spacing between the particles decreases (compression), and tends to decrease when the spacing between the particles increases (rarefaction). By differentiating (2.6) twice in respect to time, one achieves:

$$\frac{\partial^2 \rho_w}{\partial t^2} = -\rho_0 \frac{\partial}{\partial x} \frac{\partial^2 \xi_x}{\partial t^2}. \quad (2.7)$$

After substituting (2.7) into (2.3), while assuming  $\rho \approx \rho_0$ , one obtains:

$$\frac{\partial^2 \rho_w}{\partial t^2} - \frac{\partial^2 P}{\partial x^2} = 0. \quad (2.8)$$

Since the instantaneous pressure is  $P = P_0 + P_w$ , and under the assumption that  $P_0$  is uniform along the  $x$  axis, then  $\frac{\partial^2 P}{\partial x^2} = \frac{\partial^2 P_w}{\partial x^2}$ , which leads to:

$$\frac{\partial^2 \rho_w}{\partial t^2} - \frac{\partial^2 P_w}{\partial x^2} = 0. \quad (2.9)$$

In order to derive the final form of the wave equation, a relationship between  $\rho_w$  and  $P_w$  is needed. The instantaneous pressure  $P$  can be estimated by the following Taylor's expansion:

$$P(\rho) = P_0 + \left( \frac{\partial P}{\partial \rho} \right)_{\rho_0} (\rho - \rho_0) + \frac{1}{2} \left( \frac{\partial^2 P}{\partial \rho^2} \right)_{\rho_0} (\rho - \rho_0)^2 + \dots \quad (2.10)$$

Assuming a linear regime, condition satisfied when the pressure fluctuations are small enough so that  $P_w \ll P_0$ , second and higher order terms of (2.10) can be neglected. This gives a linear relationship between the pressure and density fluctuation:

$$P_w = \mathcal{B} \frac{\rho_w}{\rho_0}, \quad (2.11)$$

where  $\mathcal{B} = \rho_0 \left( \frac{\partial P}{\partial \rho} \right)_{\rho_0}$  is the adiabatic bulk modulus. After substituting (2.11) into (2.9) one obtains the wave equation for the acoustic pressure:

$$\frac{1}{c^2} \frac{\partial^2 p}{\partial t^2} - \frac{\partial^2 p}{\partial x^2} = 0, \quad (2.12)$$

where  $p$  is commonly used to refer to the pressure fluctuations  $P_w$ , and  $c = \sqrt{\frac{\mathcal{B}}{\rho_0}}$  is the speed of sound in the medium. In a three-dimensional space, (2.12) can be rewritten as:

$$\boxed{\frac{1}{c^2} \frac{\partial^2 p}{\partial t^2} - \nabla^2 p = 0.} \quad (2.13)$$

Equation (2.13) is a constitutional equation in linear acoustics, describing the propagation of a pressure perturbation within a medium.

A general solution of a harmonic plane wave travelling along the  $x$  direction is:

$$\mathbf{p} = \mathbf{p}_+ + \mathbf{p}_- = \mathbf{A}e^{j(\omega t - kx)} + \mathbf{B}e^{j(\omega t + kx)}, \quad (2.14)$$

where  $\mathbf{p}$  is the complex pressure,  $\mathbf{p}_+$  and  $\mathbf{p}_-$  denote a wave travelling in the positive and negative  $x$  direction, respectively.  $\mathbf{A}$  and  $\mathbf{B}$  are the complex amplitudes of the pressure waves,  $\omega$  is the angular frequency and  $k$  is the wave number. Since the most important property of (2.13) is that it is linear, Equation (2.14), which is the sum of two solutions, is also a solution of the wave equation. More generally, a solution for a plane wave traveling in space can be expressed as:

$$\mathbf{p} = \mathbf{A}e^{j(\omega t - \vec{k} \cdot \vec{r})}, \quad (2.15)$$

where  $\vec{k} = k_x \hat{x} + k_y \hat{y} + k_z \hat{z}$  is the wave vector, and  $\vec{r} = x \hat{x} + y \hat{y} + z \hat{z}$  is the position vector. A general solution for a spherical wave can be written as:

$$\mathbf{p} = \frac{\mathbf{A}}{r} e^{j(\omega t - kr)}, \quad (2.16)$$

where  $r$  denotes the distance from the origin in a polar coordinate system, the sound point source being located at the origin. It can be noted that, unlike for plane waves, the amplitude of a spherical pressure wave is not constant, but inversely proportional to the propagation distance.

## 2.1.2 Reflection and transmission of sound

When a travelling wave encounters a discontinuity between two different media, reflected and transmitted waves can be generated at their boundary. Although, for a normal incident wave, same equations derived for fluids may apply in the case one of the media is a solid, since solids can sustain different modes of propagation other than longitudinal waves, complications might arise in the case the incident wave is not normal to the plane separating the two media. For simplicity, in this section all media are assumed to be fluids. Let  $z_1 = \rho_1 c_1$  and  $z_2 = \rho_2 c_2$  be the acoustic impedance of two different media, medium 1 and medium 2, respectively, and let the plane  $x = 0$  be the interface between them. Assuming a plane wave travelling from medium 1 to medium 2 in the direction normal to the plane  $x = 0$ , let  $\mathbf{p}_i$  be the incident wave propagating in medium 1, expressed as:

$$\mathbf{p}_i = \mathbf{P}_i e^{j(\omega t - k_1 x)}, \quad (2.17)$$

where the subscript "1" refers to properties of medium 1. When the incident wave  $\mathbf{p}_i$  reaches the plane  $x = 0$ , a reflected wave  $\mathbf{p}_r$ , traveling along the

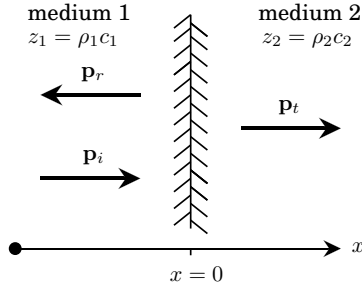


**Figure 2.3.** Reflection and transmission of a plane wave at the interface between two media.

negative  $x$  direction in medium 1, is generated at the boundary

$$\mathbf{p}_r = \mathbf{P}_r e^{j(\omega t + k_1 x)}, \quad (2.18)$$

and a transmitted wave traveling in the positive  $x$  direction is generated in medium 2

$$\mathbf{p}_t = \mathbf{P}_t e^{j(\omega t - k_2 x)}. \quad (2.19)$$

Since there cannot be any net force generated at the interface, one can write the following condition:

$$\mathbf{p}_i + \mathbf{p}_r = \mathbf{p}_t, \quad (2.20)$$

which is also known as *continuity of pressure*. Since the media are expected to be in contact at  $x = 0$ , the condition of *continuity of normal velocity* states that normal component of the velocity must be equal at both sides of the interface:

$$\mathbf{v}_i + \mathbf{v}_r = \mathbf{v}_t, \quad (2.21)$$

where  $\mathbf{v}_i$  and  $\mathbf{v}_r$  are the particle velocities of medium 1 at  $x = 0$  due to the incident and reflected wave, respectively, and  $\mathbf{v}_t$  is the particle velocity of medium 2 due to the transmitted wave. By dividing (2.20) and (2.21) one obtains:

$$\frac{\mathbf{p}_i + \mathbf{p}_r}{\mathbf{v}_i + \mathbf{v}_r} = \frac{\mathbf{p}_t}{\mathbf{v}_t}. \quad (2.22)$$

For plane waves, the acoustic impedance can be expressed as  $z = \pm \frac{\mathbf{p}}{\mathbf{v}}$ , where the sign is justified on whether the wave is traveling in the positive (+) or negative (−) axis direction. Accordingly, by rewriting (2.22) in function of  $\frac{\mathbf{p}_r}{\mathbf{p}_i}$ , one has:

$$\mathbf{R} = \frac{\mathbf{p}_r}{\mathbf{p}_i} = \frac{z_2 - z_1}{z_1 + z_2}. \quad (2.23)$$

The term  $\mathbf{R}$  is commonly referred to as the reflection coefficient, describing the ratio of a wave being reflected at a boundary. The ratio of wave

being transmitted to medium 2 is described by the transmission coefficient  $\mathbf{T} = \frac{\mathbf{p}_t}{\mathbf{p}_i}$ , which is also defined as:

$$\mathbf{T} = 1 + \mathbf{R}. \quad (2.24)$$

Considering a plane wave striking the interface at  $x = 0$  and forming an

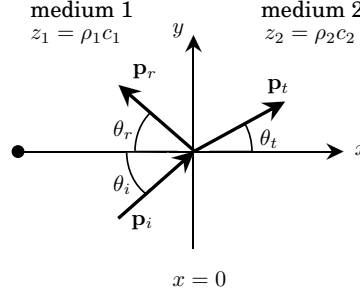


**Figure 2.4.** Reflection and transmission of an oblique incident plane wave at the interface between two media.

angle  $\theta_i$  in respect to the  $x$ -axis, the wave vector describing the direction of the incident wave within the  $xy$ -plane can be expressed as:

$$\vec{k} = k_x \hat{x} + k_y \hat{y}, \quad (2.25)$$

$$k_x = \vec{k} \cdot \hat{x} = k_1 \cos \theta_i \quad (2.26)$$

$$k_y = \vec{k} \cdot \hat{y} = k_1 \sin \theta_i. \quad (2.27)$$

Therefore, the incident plane wave can be written as:

$$\mathbf{p}_i = \mathbf{P}_i e^{j(\omega t - k_1 x \cos \theta_i - k_1 y \sin \theta_i)}, \quad (2.28)$$

and similarly for the reflected and transmitted wave:

$$\mathbf{p}_r = \mathbf{P}_r e^{j(\omega t + k_1 x \cos \theta_r - k_1 y \sin \theta_r)}, \quad (2.29)$$

$$\mathbf{p}_t = \mathbf{P}_t e^{j(\omega t - k_2 x \cos \theta_t - k_2 y \sin \theta_t)}. \quad (2.30)$$

where the angle of the transmitted wave,  $\theta_t$ , can be a complex number depending on the angle of the incident wave. Since condition (2.20) must be met for  $x = 0$ , one can write:

$$\mathbf{P}_i e^{-jk_1 y \sin \theta_i} + \mathbf{P}_r e^{-jk_1 y \sin \theta_r} = \mathbf{P}_t e^{-jk_2 y \sin \theta_t}, \quad (2.31)$$

which, in order to be satisfied for  $-\infty < y < +\infty$ , implies that:

$$k_1 \sin \theta_i = k_1 \sin \theta_r = k_2 \sin \theta_t. \quad (2.32)$$

From (2.32) it follows that  $\theta_i = \theta_r$  which means that the angle formed by the reflected wave is equal to the one formed by the incident wave. Moreover, it follows that:

$$\frac{\sin \theta_i}{c_1} = \frac{\sin \theta_t}{c_2}, \quad (2.33)$$

which is also known as the Snell's law, where  $c_1$  and  $c_2$  are the speed of sound in medium 1 and medium 2, respectively. By taking into consideration the trigonometric identity, one can note that:

$$\cos \theta_t = \sqrt{1 - \sin^2 \theta_t} = \sqrt{1 - \left(\frac{c_2}{c_1}\right)^2 \sin^2 \theta_i}, \quad (2.34)$$

which, depending on the angle of incidence  $\theta_i$ , can have either complex or real solutions. In order for (2.34) to be a real number, the following condition must be satisfied:

$$\sin \theta_i \leq \frac{c_1}{c_2}. \quad (2.35)$$

If  $c_1 > c_2$ , condition (2.35) is met and (2.34) is a real number for  $0 < \theta_i < \frac{\pi}{2}$ . If  $c_1 < c_2$ , condition (2.35) is true only if

$$\theta_i \leq \theta_c = \arcsin \frac{c_1}{c_2}, \quad (2.36)$$

where  $\theta_c$  is defined as the *critical angle*. If  $c_1 < c_2$  and  $\theta_i \geq \theta_c$ , (2.34) can be expressed in following complex form:

$$\cos \theta_t = \pm j \sqrt{\left(\frac{c_2}{c_1}\right)^2 \sin^2 \theta_i - 1}. \quad (2.37)$$

and by substituting (2.37) into (2.30), the transmitted plane wave can be written as:

$$\mathbf{p}_t = \mathbf{P}_t e^{j(\omega t \pm j k_2 x \sqrt{\left(\frac{c_2}{c_1}\right)^2 \sin^2 \theta_i - 1} - k_2 y \sin \theta_t)} = \mathbf{P}_t e^{\pm \gamma x} e^{j(\omega t - k_1 y \sin \theta_i)}, \quad (2.38)$$

where  $\gamma$  is defined as:

$$\gamma = k_2 \sqrt{\left(\frac{c_2}{c_1}\right)^2 \sin^2 \theta_i - 1}. \quad (2.39)$$

It can be seen from (2.38) that, when  $c_1 < c_2$  and  $\theta_i \geq \theta_c$ , the transmitted wave propagates along the  $y$  direction, parallel to the interface, and with decreasing or increasing amplitude along the  $x$  direction, perpendicular to the interface. However, the positive root of (2.38) would mean the wave amplitude will increase infinitely along the positive  $x$  direction, which is physically impossible. Therefore, only the negative root of (2.38) is acceptable and the wave will propagate along the  $y$  direction with decaying amplitude along the positive  $x$  direction.

### 2.1.3 Attenuation of sound

Normally, the intensity of acoustic waves decreases as they propagate through a medium. This phenomenon is known as *attenuation of sound* and it can be caused by several factors, such as the geometric spreading of a sound wave, scattering and absorption mechanisms (*i.e.*, thermal losses, viscous losses, hysteresis). Considering a plane wave travelling along the positive  $x$  direction, the attenuation effects can be accounted for as:

$$\mathbf{p} = P_0 e^{-\alpha x} e^{j(\omega t - kx)}, \quad (2.40)$$

where  $P_0$  is the pressure amplitude at the source located at  $x = 0$ , and  $\alpha$  ( $\text{cm}^{-1}$ ) is the attenuation coefficient. Since the overall attenuation is the result of different absorption mechanisms contributing to the reduction of the pressure wave amplitude, when losses are small, the attenuation coefficient can be expressed as [60]:

$$\alpha = \sum_i \alpha_i, \quad (2.41)$$

where  $\alpha_i$  accounts for the individual loss mechanisms.

#### *Attenuation due to geometric spreading*

Assuming lossless medium, the total power  $W_T$  carried by the sound waves remains constant, while the instantaneous intensity  $I$  may decrease farther away from the source. For example, if one considers spherical waves, the intensity decreases as a function of the distance  $r$  from a monopole point source located at  $r = 0$ , because the same power  $W_T$  is being distributed over greater areas. Let  $W_1$  and  $W_2$  be the powers calculated at the surfaces  $S_1$  and  $S_2$  having radii  $r_1$  and  $r_2$ , respectively. Since there are no losses, the conservation of power applies so that:

$$W_1 = W_2 \rightarrow I_1 S_1 = I_2 S_2 \rightarrow I_1 4\pi r_1^2 = I_2 4\pi r_2^2 \rightarrow I_1 r_1^2 = I_2 r_2^2. \quad (2.42)$$

From (2.42) it follows that  $I_2 = I_1 \frac{r_1^2}{r_2^2}$ , therefore the intensity decreases as a function of  $\frac{1}{r^2}$ . Consequently, since  $I \propto p^2$ , the pressure decreases as  $\frac{1}{r}$ . In the case of a line sound source with length  $H$ , the emitted sound waves propagate as cylindrical waves. Similarly to (2.42), assuming that the boundary effects are negligible, one can write the following:

$$I_1 2\pi r_1 H = I_2 2\pi r_2 H \rightarrow I_1 r_1 = I_2 r_2. \quad (2.43)$$

Conversely to spherical waves, the acoustic intensity of cylindrical waves decreases as a function of  $\frac{1}{r}$ , therefore, the pressure must decrease as a function of  $\frac{1}{\sqrt{r}}$ .

*Attenuation due to scattering*

Scattering occurs when a travelling sound wave encounters some inhomogeneities in a material, such as particles with different shapes and material properties, usually called scatterers. If the wavelength  $\lambda$  of the sound beam is much smaller than the characteristic size  $a$  of the particle, the scattered wave can be derived by applying the laws of reflection of a sound wave at the interface of a material discontinuity. However, if  $\lambda \sim a$ , the expression for the scattered wave becomes more difficult to derive, and it depends on the scatterer shape and its impedance mismatch with the surrounding medium. The overall attenuation of sound would arise from the multiple reflections caused by the interaction of the wave and the scatterers, which results in deviating part of the acoustic energy carried by the main sound beam.

*Attenuation due to viscous losses*

When an acoustic wave travels through a viscous fluid, the wave can be subject to attenuation due to viscous losses, *i.e.*, absorption. These losses are attributable to the relative motion between adjacent fluid layers, which can lead to the conversion of acoustic energy into other forms of energy (*e.g.*, thermal energy). The complex wave vector  $\mathbf{k}$  accounting for the viscous losses can be obtained by considering the following lossy wave equation:

$$\left(1 + \tau_s \frac{\partial}{\partial t}\right) \nabla^2 p = \frac{1}{c_0^2} \frac{\partial^2 p}{\partial t^2}, \quad (2.44)$$

where  $\tau_s = (\frac{4}{3}\eta + \eta_B)/\rho_0 c_0^2$  is the relaxation time, derived by linearizing the Navier–Stokes equation, being  $\eta$  the coefficient of shear viscosity and  $\eta_B$  the coefficient of bulk viscosity. The time harmonic representation of (2.44) leads to:

$$\nabla^2 \mathbf{p} + \mathbf{k}^2 \mathbf{p} = 0, \quad (2.45)$$

where  $\mathbf{k}$  is the complex wave vector defined as:

$$\mathbf{k} = \frac{\omega}{c_0(1 + j\omega\tau_s)^{\frac{1}{2}}}. \quad (2.46)$$

By separating (2.46) into its real and imaginary part:

$$\mathbf{k} = k - j\alpha_s, \quad (2.47)$$

$$\alpha_s \approx \frac{1}{2} \frac{\omega^2}{c_0} \tau_s, \quad (2.48)$$

$$c_p = \frac{\omega}{k} \approx c_0 \left[1 + \frac{3}{8} (\omega\tau_s)^2\right], \quad (2.49)$$

with  $\alpha_s$  being the absorption coefficient due to viscous losses, and with  $c_p$  being the phase velocity. It can be noted that absorption is a function of  $\omega^2$ , meaning that viscous losses effect increase rapidly with the frequency. Moreover, the phase velocity is not constant, but is also a function of the frequency, meaning that the propagation of sound waves in viscous fluids is dispersive [60].

#### *Attenuation due to thermal effects*

When an acoustic wave travels through a thermally conducting medium, it is possible to observe a local increase in temperature during the compression phase of the sound wave. This results in generating a temperature gradient within the medium, which causes the molecules to diffuse from hotter regions, associated with higher kinetic energy, to cooler regions. This migration process is responsible for transforming part of the acoustic energy into thermal energy, hence constituting an absorption mechanism due to thermal effects [36, 61, 62].

#### *Attenuation due to hysteresis*

Sound attenuation due to hysteresis effects may arise when there is a lag between the applied stress and the resulting strain taking place in a material. Due to this phenomenon, the relationship between stress and strain is not linear and it may depend on whether the material is being compressed or stretched. As a consequence, the work done by the material during one full cycle is non-zero, suggesting that a portion of the acoustic energy is dissipated into other forms of energy (*e.g.*, thermal energy) [63, 62].

## **2.2 Non-Linear Ultrasound**

At high pressure levels, the propagation of US waves in a medium might become non-linear. As the total acoustic power (TAP) increases, the ultrasonic waves start interacting with the medium they are travelling in, inducing the formation of non-linear phenomena that can alter the acoustic material properties. Such alterations might affect the propagation of US waves, which cannot be described with the linear acoustic wave equation derived in the previous section.

At high pressure amplitudes the relation between pressure, velocity and density is not linear, and second and higher terms that appear in (2.10)

cannot be neglected. The equation of state can be written as:

$$P - P_0 = A \frac{\rho - \rho_0}{\rho_0} + \frac{B}{2} \left( \frac{\rho - \rho_0}{\rho_0} \right)^2 + \dots, \quad (2.50)$$

where:

$$A = \rho_0 \left( \frac{\partial P}{\partial \rho} \right)_{\rho_0}, \quad (2.51)$$

$$B = \rho_0^2 \left( \frac{\partial^2 P}{\partial \rho^2} \right)_{\rho_0}. \quad (2.52)$$

The terms  $A$  and  $B$  are used to characterize the strength of non-linearities in a medium, and their relation  $B/A$  is usually referred to as the *non-linearity parameter*.

High intensity ultrasound (HIU) is often used in applications where the intent is to induce an effect in the medium through which the wave propagates. These effects include the potential formation of NLU phenomena, such as acoustic radiation pressure, acoustic streaming, cavitation, which have been widely studied and used in different medical applications. However, HIU is not always a prerequisite for inducing NLU effects, as material nonlinearities and geometric discontinuities may also contribute to giving rise to NLU phenomena.

### 2.2.1 Acoustic radiation force

An ARF acting on a surface of an object can be observed when a non-focused ultrasonic pressure wave, travelling in a fluid with speed of sound  $c$ , impinges on the surface of such object. It is defined as a time average force that arises from the momentum transfer from the incident wave to the object, and it is expressed as [64]:

$$F_{rad} = d_r \langle E_{ac} \rangle S, \quad (2.53)$$

where  $\langle E_{ac} \rangle$  is the Langevin radiation pressure (Pa),  $S$  is the surface of the object the sound wave is impinging ( $\text{m}^2$ ) and  $d_r$  (dimensionless unit) is the drag coefficient. For a harmonic plane wave normally impinging on a perfect absorber, the Langevin radiation pressure can be expressed as the time-averaged energy density:

$$P_{Lan} = \langle E_{ac} \rangle = \frac{p_0}{2\rho_0 c^2} = \frac{I}{c}, \quad (2.54)$$

where  $p_0$  is the pressure amplitude,  $\rho_0$  the density,  $c$  the speed of sound and  $I$  the intensity of the wave. The drag coefficient  $d_r$  describes the amount of

scattering of absorption of a wave impinging onto the surface of an object, and it is defined for unity energy density of the incident wave. It can be expressed as [65]:

$$d_r = 1/s \left( \Pi_a + \Pi_s - \int \gamma \cos \theta dA \right) - i/s \int \gamma \sin \theta dA. \quad (2.55)$$

In the above,  $\Pi_a$  and  $\Pi_s$  represent the total power absorbed and scattered by the object, respectively. The term  $s$  is the projected area of the object, while  $\gamma$  is the intensity of the scattered wave and  $\theta$  is the angle formed by the incident wave with the scattered wave. If the object is a perfect absorber with axis of symmetry parallel to the normal of the incident wave, the drag coefficient will be equal to 1. If the object is a perfect reflector, the drag coefficient will be equal to 2.

### 2.2.2 Acoustic streaming

The acoustic streaming is the steady motion of homogeneous fluid due to the momentum transfer from an acoustic wave to the fluid [66]. It is mainly caused by sound attenuation of the medium due to the absorption of acoustic energy and requires non-linearity in the equation of the motion of the medium. The acoustic streaming in a fluid is driven by the following time-averaged volume force:

$$F = \langle \rho_f \frac{\partial \mathbf{v}}{\partial t} \rangle + \rho_f \langle (\mathbf{v} \cdot \nabla) \mathbf{v} \rangle, \quad (2.56)$$

where  $\rho_f$  is the density perturbation of the fluid and  $\mathbf{v}$  is the acoustic velocity. As the time average of a quadratic periodic variable is nonzero, the driving force  $F$  responsible for the acoustic streaming generation will be always nonzero, when an acoustic wave is travelling in a fluid. The streaming can manifest as a bulk flow, which arises from the attenuation of the US wave as it propagates through a medium. This type of streaming is called Eckart streaming and it is more intense at high frequencies (MHz), as sound absorption mechanisms become more relevant at increased frequencies [67, 68, 69].

In an acoustic standing wave field, the streaming generated close to an oscillating boundary is called Rayleigh–Schlichting streaming, and it usually takes place on a smaller length scale compared to the Eckart streaming. The Schlichting streaming originates as vortices within the boundary layer thickness, and it is characterized by a net motion of fluid oriented from the pressure antinodes to the pressure nodes close to the oscillating boundary [70]. It is mainly caused by greater viscous dissipation

occurring in this region as compared to in the bulk fluid, due the high velocity gradient normal to the solid surface generated by the presence of the non-slip boundary between the liquid phase and the solid. The Rayleigh streaming instead develops in the outer boundary layer, and it manifests as streaming vortices rotating in the opposite direction than that of the Schlichting streaming [71].

### 2.2.3 Cavitation

Acoustic cavitation is a phenomenon arising from the interaction of spherical bubbles and ultrasonic pressure waves travelling in a fluid. Pre-existing small bubbles, formed by gas dissolved in the fluid, are made to expand when the local pressure becomes lower than the internal pressure of the bubble, and to be compressed when the local pressure is greater than the pressure inside the bubble. If the pressure amplitude of the external acoustic field is sufficiently low, the bubbles can oscillate around their equilibrium radius in a predictable way. This type of cavitation is usually referred to as *stable* or *non-inertial cavitation* (Figure 2.5a,b). However, at high acoustic intensities, if the local pressure falls below a certain cavitation threshold [72] the bubbles can grow up several times their original diameter, and consequently collapse, when the pressure becomes positive [73].

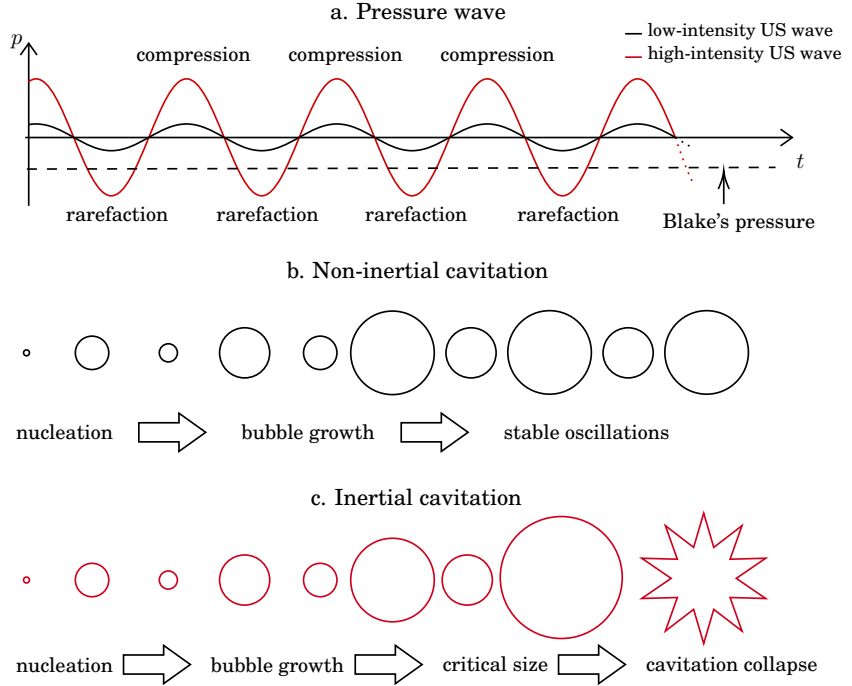


**Figure 2.5.** Schematics describing a non-inertial and inertial cavitation event.

This type of cavitation is instead called *transient* or *inertial cavitation* (Figure 2.5c). The collapse is so violent that temperatures of thousands of kelvin are reached inside the collapsing bubble, acoustic emission in the form of shockwaves can be generated and, eventually, emission of light (sonoluminescence) can be also observed [74].

The size of a bubble that resonates with the applied frequency is predicted by [75]:

$$R = \sqrt{\frac{3\gamma P_\infty}{\rho_f \omega}}, \quad (2.57)$$

where  $R$  is the radius of the bubble at rest,  $\gamma$  is the specific heat ratio of the gas inside the bubble,  $P_\infty$  the ambient liquid pressure,  $\rho_f$  the liquid density and  $\omega$  the angular frequency. The cavitation threshold criterion is governed by the Blake's pressure [76], which determines the critical negative pressure below which a cavitation event will occur:

$$P_B = P_\infty + \frac{8\sigma}{9} \sqrt{\frac{3\sigma}{2R_B^3(P_\infty + (2\sigma/R_B))}}, \quad (2.58)$$

where  $P_B$  is the Blake pressure,  $\sigma$  is the surface tension and  $R_B$  is the Blake bubble radius.

### 2.2.4 Shockwaves

Shockwaves are large pressure perturbations travelling faster than the local speed of sound, and are characterized by discontinuous changes in density, pressure and particle velocity along the propagation front [77]. Shockwaves can arise due to non-linearities of the medium, which can contribute to distortion of the travelling wave [78]. In fact, at high pressure levels the acoustic properties of the medium are momentarily changed, resulting in the compressional phase of the wave traveling faster than the rarefactional phase. Eventually, an abrupt change in pressure will occur, and shockwaves will be generated. For a lossless plane, the *discontinuity distance*  $\ell$ , which is the distance from the sound source at which a shock front is generated, can be calculated as [79]:

$$\ell = 1/\beta Mk, \quad (2.59)$$

where  $M$  is the Mach number, which is the ratio between the particle velocity and the speed of sound,  $\beta = 1 + B/2A$  is the coefficient of non-linearity, and  $k$  is the wave number. However, at high frequencies the presence of losses might considerably attenuate the strength of the pressure wave before it reaches the discontinuity distance. This effect is described by the Gol'dberg number [80]:

$$\Gamma = 1/\alpha\ell, \quad (2.60)$$

where  $\alpha$  is the absorption coefficient. If  $\Gamma < 1$ , the pressure wave will vanish before reaching the discontinuity distance, while, if  $\Gamma > 1$ , the non-linearities of the medium will take over and a shockwave will be generated at the discontinuity distance  $\ell$ .

Shockwaves might also arise from implosion of cavitating bubbles. During the collapse, the inward motion of the bubble wall is swiftly inverted, creating discontinuities in the pressure field and particle velocity in the surroundings of the bubble wall. Under these conditions, a spherical shockwave might be formed [81, 82].

## 3. Methods

This section describes the instrumentation and the methods developed for the work presented in this Thesis.

### 3.1 Experimental Arrangements

#### 3.1.1 Ultrasonic device

A custom-made ultrasonic device has been developed and used for the experiments (Figure 3.1) (Publications I–III). A Langevin US transducer, with a natural frequency of 40 kHz was used as the sound source of the prototype. The horn of the transducer is coupled to a solid 3D printed aluminum waveguide (3D Step Oy, Ylöjärvi, Finland) via a screw-tightening system. The serpentine shape of the waveguide was selected to convert the longitudinal motion, provided by the distal part of the transducer, to a flexural motion at the end of its tapered structure. The cross-sectional area of the distal portion of the waveguide was designed with an exponential tapering in order to minimize reflections and provide amplified displacements at its tip. A hole of 0.8 mm was drilled along the center line of the tip of the waveguide in order to accommodate a 21G×80 mm hypodermic needle (model: 4665465, 100 STERICAN, B Braun, Melsungen, Germany). The coupling point between the needle and the waveguide was chosen to match a displacement anti-node in the needle structure, located at  $3\lambda = 45$  mm from the needle tip, considering a standing wave at the frequency of 33 kHz being generated in the needle. A vacuum source, for example a 10 mL syringe (catalogue number: 12931031, Plastic PP Syringes Luer Slip, Fisherbrand, Fisher Scientific, Hampton, NH, United States), was employed in order to draw or deliver material through the needle.

## Device schematics

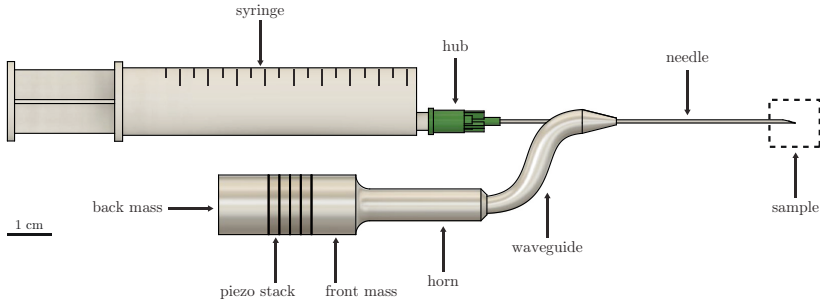


**Figure 3.1.** Schematic depicting the custom-made ultrasonic device employed in the experiments.

### 3.1.2 Electronics

The ultrasonic device was powered by a RF power amplifier (model: AG 1012LF, Amplifier/Generator, T&C Power Conversion, Inc., Rochester, NY, United States) and a function generator (model: Analog Discovery 2, Digilent, Inc., Henley Court Pullman, WA, United States), which provided the driving signal (Publications I–III). Since the impedance of the ultrasonic device and of the power amplifier are different at the employed frequency of 33 kHz, an impedance matching circuit was designed in order to maximize the power transmission from the source to the load. By theory, the maximum output power is delivered to the load when the following condition is satisfied [83]:

$$Z_0 = Z_L^*, \quad (3.1)$$

where  $Z_0$  is the impedance of the source and  $Z_L^*$  denotes the complex conjugate of the load impedance. The resistance of the load was matched to the  $50 \Omega$  the amplifier by building a transformer with turns ratio equals to:

$$\frac{n_2}{n_1} = \sqrt{\frac{R_L}{R_0}} = 10 : 1, \quad (3.2)$$

where  $n_1$  is the number of coil turns on the primary winding,  $n_2$  is the number of coil turns on the secondary winding,  $R_L$  is the resistance of the load and  $R_0$  is the resistance of the amplifier, which amounts to  $50 \Omega$ .

### 3.1.3 Optics

The main optical method used during the work of this Thesis was high-speed (HS) imaging. A Phantom V1612 camera (Vision Research, Wayne, NJ, United States) was used in combination with a macro lens (model:

Canon MP-E 65 mm f / 2.8 1-5× Macro Photo, Canon Inc., Ōta, Tokyo, Japan) or a general purpose lens (model: Canon EF-S 15-85 mm f / 3.5-5.6 IS USM, Canon Inc.), depending on the length scale of the phenomenon to be investigated (Publications I–III). A white light-emitting diode (catalogue number: 4052899910881, White Led, 3000 K, 4150 lm, Osram Opto Semiconductors, Germany) (Publications I and II) and a halogen fiber optic illuminator (model: OSL2IR, High-Intensity Fiber-Coupled Illuminator, Thorlabs, Inc., Newton, NJ, United States) (Publication III), were used as light sources to produce back-lit shadowgraph images of the needle motion inside the medium.

Other optical methods used were the Schlieren photography, which was designed and assembled in order to visualize the density perturbation of the fluid surrounding the ultrasonically actuated needle (details of the setup provided in Publication I), the optical projection tomography (OPT), performed with an OPT scanner (Bioptics OPT 3001M Scanner), and microscopy imaging of histological slides (3DHISTECH Panoramic 250 FLASH II).

### 3.1.4 Software

MATLAB (R2020b) [84] was used as the main programming platform for the analysis of raw experimental data and development of automation algorithms. Numerical simulations of the NLU phenomena were performed in COMSOL Multiphysics v5.5 [85], while Fusion 360 was used as CAD modelling tool.

Several algorithms have been developed to analyse in a quantitative manner the collected experimental data. For example, a method employing image registration of consequent HS images of the cavitation activity in water via cross-correlation in the frequency domain [86] was used to detect the needle position over time and to quantify the projected area of cavitation activity. A more extensive description of this method is provided in Publication I. A modified version of this method was also used to segment the cavitation activity boundaries from HS images, when needle was actuated in thin sections of *ex-vivo* bovine liver (description of the method provided in Publication III). The velocity maps the direction and magnitude of the fluid motion have been produced by analysing the HS footages with an algorithm that uses a similar approach to that used in particle image velocimetry (PIV) [87] (description provided in Publication I).

### 3.1.5 Samples

First, deionized and degassed water ( $5.8 \text{ mg L}^{-1}$ ) was employed in the experiments in order to study the interaction between the oscillating needle and well-known matter, and to optically confirm the generation of NLU phenomena such as cavitation, atomization and acoustic streaming (Publication I). The action of these phenomena in water was easily quantified through HS imaging (section 3.1.3) and image analysis (section 3.1.4).

Ballistic gelatin (10% w/v porcine gelatin/deionized water) was chosen as an appropriate model to investigate the mechanical effects of the needle on a soft-tissue-like material. Importantly, its acoustic impedance is close to that of soft tissue, and it has been used in several studies as an US phantom to explore the cavitation-induced damage mechanism in soft-tissue-like models [88]. The protocol for preparing the ballistic gelatin sample used in the experiments is accurately described in Publication I.

In order to investigate the translation of nanoparticles and fluids inside porous media promoted by the needle action, hydrogels with different agarose concentrations (0.5, 1 and 2%; w/v agarose powder/EDTA) were used in the experiments. Agarose gel was selected because its rheological properties (*e.g.*, porosity, permeability) can be controlled so that they closely match those of some soft tissues. A protocol for preparing the hydrogel samples used in this study is proposed and described in Publication II.

Different *ex vivo* bovine tissues, such as liver, kidney, spleen and striated muscle were used to demonstrate the influence of the oscillating needle on soft tissue, exemplified by performing USeFNABs at different TAP levels (0.2, 0.5 and 0.8 W). In Publication I, an extensive description of the biopsy procedure, sample weighing, and of the protocol for processing the biopsy samples in histological sections is provided. In a separate experiment, thin slices ( $\sim 1 \text{ mm}$ ) of bovine liver tissue were subjected to sonication with the ultrasonic needle, with the intent of directly visualizing cavitation events generated inside soft tissue enabled by HS imaging. All specimens were retrieved from the slaughterhouse (Vainion Teurastamo Oy, Orimattila, Finland) within 1–2 h *post mortem* and experiments were always performed within 6 h *post mortem* at room temperature (22–24 °C). The equipment used for preparing the samples into thin sections, and setup used during the experiments is described in detail in Publication III.

## 3.2 Numerical Simulations

Numerical modeling was used to study and deepen the understanding of the NLU phenomena generated by the ultrasonically actuated needle. In the following, a general overview of the numerical methodology used to simulate the ultrasonic actuation of a medical needle and ultrasonic related phenomena generated by the oscillating needle in different media is presented.

### 3.2.1 Geometry and materials

First, the ultrasonic device geometry was replicated in Fusion 360 and the 3D model was imported into the COMSOL Multiphysics environment. The piezo-stack of the Langevin transducer consisted of four piezoelectric ceramic rings (length = 2.5 mm, diameter = 15 mm, material = lead zirconate titanate PZT-5H). The back mass (length = 15 mm, diameter = 15 mm), the front mass (length = 8.5 mm, diameter = 15 mm) and the horn (length = 31 mm, diameter = 8 mm) were assumed to be made of stainless steel, while the waveguide was made of aluminium. The needle was modelled as a hollow cylinder (outer diameter = 0.819 mm, inner diameter = 0.514 mm, length 80 mm) made of stainless steel. The needle tip geometry was modelled with a bevel angle  $\xi$  of 12.92°, secondary bevel angle  $\varphi$  of 20.59° and angle of rotation  $\beta$  of 58° [89]. The parameters  $\xi$ ,  $\varphi$  and  $\beta$ , which define the needle cutting edge geometry, were determined experimentally by visualizing the tip of a 21G hypodermic needle with a microscope. The sample domain has been modeled as a cylinder with different material properties (*i.e.*, water, agarose gel, liver) depending on the medium where the acoustic phenomenon is assumed to take place (Publications II and III).

### 3.2.2 Needle motion

The displacement of the needle was calculated in the frequency domain by solving the linear elastic equation of motion [90] within the ultrasonic arrangement:

$$\rho \frac{\partial^2 \mathbf{u}}{\partial t^2} = \nabla \cdot \mathbf{T} + \mathbf{F}_m, \quad (3.3)$$

where  $\rho$  is the density of the medium,  $\mathbf{u}$  is the displacement vector,  $\mathbf{T}$  is the Cauchy stress tensor [91] and  $\mathbf{F}_m$  represents the external volume force. In the elastic domain, the material's mechanical behavior can be expressed

through the Hooke's law:

$$\mathbf{T} = \mathbf{c} : \mathbf{S}, \quad (3.4)$$

where  $\mathbf{c}$  is the stiffness tensor,  $\mathbf{S}$  is the infinitesimal strain tensor and “:” represents the inner product. Assuming small deformations, the strain can be related to displacement as follows:

$$\mathbf{S} = \frac{1}{2}(\nabla \mathbf{u} + (\nabla \mathbf{u})^t), \quad (3.5)$$

where the superscript “t” stands for the transpose of a matrix. The wave motion within the solid structure is generated by applying an alternating potential difference across the faces of the piezoelectric rings.

### 3.2.3 Acoustic field

The propagation of acoustic waves inside medium has been modeled with linear acoustic wave equation for viscous fluids [92] (Publications II and III):

$$\nabla^2 p - \frac{1}{c_\infty^2} \frac{\partial^2 p}{\partial t^2} + \frac{\delta}{\rho_\infty c_\infty^2} \frac{\partial}{\partial t} \nabla^2 p = 0, \quad (3.6)$$

where  $p$  is the pressure,  $c_\infty$  and  $\rho_\infty$  are the speed of sound and the density of the medium, respectively. The term  $\delta$  is the sound diffusivity, which accounts for viscous losses in a viscous fluid and it is defined as [93, 94]:

$$\delta = \frac{2c_\infty^3 \alpha}{\omega^2}, \quad (3.7)$$

where  $\omega$  is the angular frequency,  $\alpha$  (1/m) is the acoustic absorption coefficient. The outer boundaries of the sample domain were assumed to be soft boundaries ( $p = 0$ ), in order to allow the pressure wave to be attenuated farther away from the needle. The structural acceleration of the portion of the needle tip is used as a boundary condition for the calculation of the acoustic pressure across the needle-sample interface as in the following mathematical condition:  $-\mathbf{n} \cdot \frac{1}{\rho_\infty} \nabla p = \mathbf{n} \cdot \mathbf{u}_{tt}$ , where  $\mathbf{u}_{tt}$  is the structural acceleration of the moving interface,  $p$  is the acoustic pressure,  $\rho$  is the density of the medium and  $\mathbf{n}$  is the vector normal to the boundary interface. This condition states that, given a positive acceleration of the interface, a negative pressure gradient is generated along the positive direction defined by  $\mathbf{n}$ .

### 3.2.4 Acoustic streaming

When simulating the interaction between the oscillating needle and fluid, whether free fluid or fluid trapped in a porous medium, the acoustic streaming [66] is assumed to be the main cause for the generation of steady fluid

flow (Publication II). In order to account for the momentum transfer from the acoustic wave to the fluid, the Reynolds stress  $\mathbf{F}$ , which represents the time-averaged volume force [95] arising from the sound attenuation in the fluid, is considered as the force term in the equations of fluid motion:

$$\mathbf{F} = -\frac{\rho}{2} \text{Re}[(\mathbf{v} \cdot \nabla) \mathbf{v}^*], \quad (3.8)$$

where  $\mathbf{v}$  is the acoustic velocity, “\*” represents the complex conjugate of a complex number and the “Re” indicates the real part. A detailed description of the acoustical and rheological properties of the porous samples modelled within the simulation environment can be found in Publication II.

### 3.2.5 Cavitation

The cavitation dynamics of a spherical gas bubble embedded in soft tissue was described by using the following Keller—Miksis equation [96]:

$$\begin{aligned} & \left(1 - \frac{\dot{R}}{c_\infty}\right) R \ddot{R} + \frac{3}{2} \left(1 - \frac{\dot{R}}{3c_\infty}\right) \dot{R}^2 = \frac{1}{\rho_\infty} \left(1 + \frac{\dot{R}}{c_\infty} + \frac{R}{c_\infty} \frac{d}{dt}\right) \times \\ & \times \left[ p_B - (p_\infty + p_f(t)) - \frac{2\sigma}{R} + J \right], \end{aligned} \quad (3.9)$$

where  $R$ ,  $\dot{R}$  and  $\ddot{R}$  denote the radial displacement, velocity and acceleration of the cavitation bubble wall, respectively. The constants  $c_\infty$  and  $\rho_\infty$  represent the speed of sound and the density of the medium. The alternating forcing pressure is expressed by  $p_f(t)$ , while the pressure at the gas-liquid interface of the bubble is defined as [97]:

$$p_B = p_0 \left(\frac{R_0}{R}\right)^{3\kappa}, \quad (3.10)$$

where  $R_0$  the bubble radius at rest and  $\kappa$  is the polytropic exponent. The term  $p_0$  represents the internal pressure of the bubble when the bubble is at equilibrium, expressed as:

$$p_0 = p_\infty + 2\frac{\sigma}{R_0}, \quad (3.11)$$

where  $p_\infty$  indicates the ambient pressure and  $S$  the surface tension of the bubble. A comprehensive description of the cavitation model used in the simulation is provided in Publication III.



## 4. Summary of publications

This chapter briefly summarizes the main results of the articles included in this Thesis.

### 4.1 Publication I

The aim of Publication I was to characterize the NLU phenomena generated by the ultrasonically actuated needle and to demonstrate its potential in the context of the biopsy application. The term *SonoLancet* (*Sono-* = sound, *-lancet* = sharp point at the very tip of the needle) was defined as the confined volume around the needle tip exhibiting pronounced interactions between the oscillating tip of the needle and the matter around it. Moreover, it was demonstrated that these interactions are highly localized at the needle tip location, hence, the SonoLancet represents a region of interest for the visualization of NLU phenomena such as cavitation, acoustic streaming, atomization and ARF.

The influence of SonoLancet on water was first studied. One experiment consisted in actuating the needle inside degassed water, while the needle action was recorded with HS imaging (300 000 fps). It was demonstrated not only the current setup is able to generate cavitation events, but also that cavitation takes place at the needle tip location and nowhere else along the needle (Figure 4.1a). This can be explained by the converging structure of the needle bevel, which causes the geometric amplification of the wave towards the needle extremity. As a consequence, large pressure fluctuations can be observed at the needle tip, resulting in cavitation activity to be more likely to take place close to its very tip, when compared to other locations along the needle shaft. Other phenomena such as ejection of microdroplets, acoustic streaming and translation of microparticles and were also observed to be more pronounced at the needle tip location (Figure

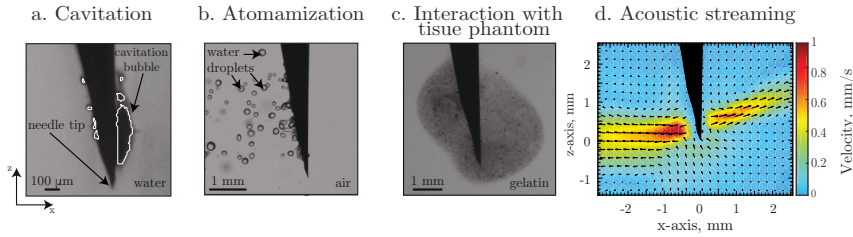


**Figure 4.1.** Example of NLU phenomena generated with the ultrasonically actuated needle. **(a)** HS frame representing a cavitation event. The needle is embedded in deionized water, and the areas enclosed within the white lines represent cavitating bubbles. **(b)** The needle is operated in air, while a small water droplet is placed at its tip. During sonication, the water droplet is broken up into several micro-droplets, whose size was inversely proportional to the driving frequency. **(c)** When the needle is operated in ballistic gelatin, cavitation activity and streaming was observed. Fluorescence nanoparticle delivered through the needle enabled visualization of the spatial distribution of the nanoparticles induced by US. **(d)** Velocity map of the acoustic streaming generated in water by the ultrasonically actuated medical needle. It can be noticed how the streaming emanates from both sides of the needle tip with directionality. These results show that the ultrasonic energy is highly concentrated at the needle tip, manifesting as formation of different NLU phenomena depending on the medium, where the needle is actuated. These NLU phenomena could potentially bring new functionalities to a standard medical needle.

#### 4.1b,c,d).

Ballistic gelatin was then used as a tissue phantom to explore these non-linear effects in conjunction with tissue-like material. When the needle was actuated inside the tissue-phantom in conjunction with fluorescent nanoparticles, generation of cavitation bubbles and acoustic streaming was optically detected (Figure 4.1c). Optical projection tomography was employed to image and reconstruct the spatial distribution of the fluorescent markers, revealing that the volume of influence of SonoLancet on phantom is localized near the needle tip. Finally, it was studied if the ultrasonic actuation of a hypodermic needle could bring benefit to the fine-needle aspiration biopsy (FNAB) procedure. The research question was motivated by the fact that a large number of FNABs are compromised due to the insufficiency of tissue extracted for diagnosis, characterized with low number or lack of pathological cells [98, 99, 100]. This can lead to inconclusive diagnoses in 9–34% of FNABs [10]. In the view of addressing this problem, it was demonstrated that, when US-enhanced fine-needle aspiration biopsies (USEFNAB) were performed in different bovine *ex-vivo* tissues (liver, spleen, kidney, striated muscle), the mass of obtained sample was increasingly improved by 3–6× compared to FNAB. The sample mass was directly proportional to the TAP involved (Figure 4.2). The results

## Mass of extracted sample as function of power

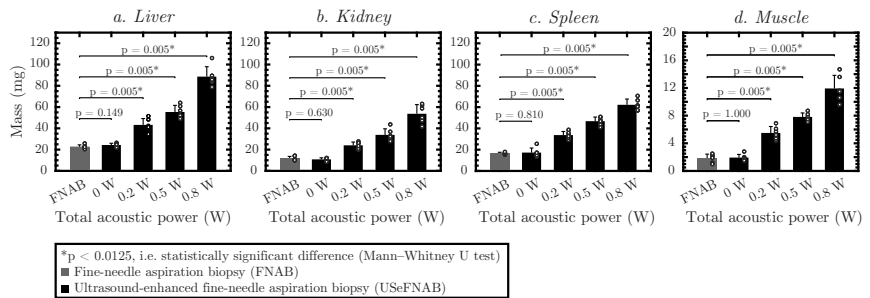


**Figure 4.2.** Mass of the extracted sample obtained from different *ex vivo* bovine tissues by using the FNABs and USEFNABs. When US energy was employed to perform the biopsies, the yield mass was increased up to 3–6 $\times$ , as compared to when FNABs were carried out.

presented in Publication I have special importance for cancer management, because it is the report in the literature to demonstrate that the ultrasonic actuation of medical needles can increase the mass of biopsy samples. Importantly, the proposed approach can mitigate the limitations associated with the FNAB application without significantly influencing the sample. Moreover, these results suggest that the NLU phenomena generated by oscillating medical needles could extend to other medical applications such as drug or gene delivery and histotripsy.

## 4.2 Publication II

Publication II demonstrated both numerically and experimentally that the ultrasonic needle can be used to translate nanoparticles and fluid within porous media. This was considered relevant for drug delivery applications in soft tissues. The study was motivated by limitations in current US mediated drug delivery systems, which mainly suffer from the inability of generating a proper ultrasonic focus at some organs inside the body, hence impacting on the delivery efficiency. For example, lesions located at the hepatic dome are difficult to treat, because the presence of ribs or air contained in the lungs represents obstacles for the sound propagation due to the acoustic impedance mismatch. However, by employing an ultrasonic needle as the sound source, one would be able to spatially bypass such anatomical structures and deliver the acoustic energy directly at the target site. Moreover, since the acoustic energy is localized at the proximity of the needle outlet, liquids or particles can be delivered to the site of US. Numerical simulations were performed in order to study the phenomenon

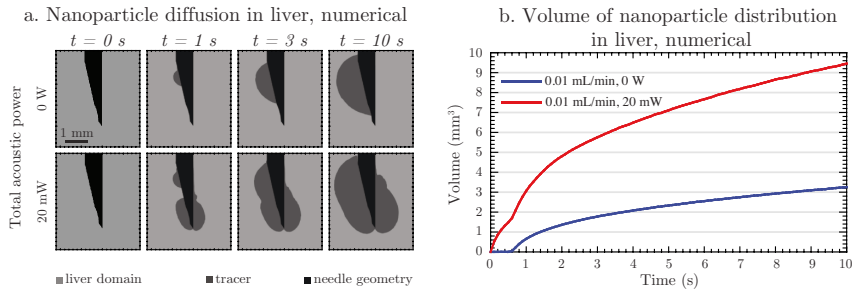


**Figure 4.3.** (a) Numerical simulation of an ultrasonically assisted injection in liver tissue. (b) When the needle is actuated at the relatively low TAP of 20 mW, the volume covered by nanoparticles is increased by three times, as compared to a standard needle injection. These results indicate that the ultrasonic action of the needle could increase the uptake of fluid caused by the enhanced delivery localized near the needle tip, which could be useful for delivering substances into tissues with compromised perfusion.

at hand. The hypothesis behind the enhanced delivery mechanism was that the needle actuation promotes the formation of acoustic streaming, which contributes to the transport of nanoparticles in porous media. For this purpose, a numerical model simulating the delivery mechanisms in agarose gel has been developed and validated experimentally. The results indicate that the ultrasonic actuation of the needle induces acoustic streaming that is highly concentrated at the proximity of the sharp edges of the needle tip. This phenomenon, which is usually referred to as sharp-edge streaming [101, 102, 103], arises from the viscous dissipation mechanisms that take place within the viscous boundary layer, resulting in the generation of strong steady flows emanating outwards along the center line of the sharp edges, which have been observed to enhance the translation of fluids and nanoparticles around the needle tip. The combined action of intense acoustic streaming (characterized by maximum velocities of  $10 \text{ mm s}^{-1}$ ) being generated at the needle tip and the enhanced convection of fluid through the interstitia of the porous medium are assumed to be the main contributor of the nanoparticle transport mechanisms. In contrast, direct ARF acting on the nanoparticles was considered to have a minor effect on the delivery, being two orders of magnitude smaller compared to ARF acting on the liquid.

The idea of providing the acoustic energy with a hypodermic needle localized at the injection site could be of use in different drug delivery applications, where the intent is to achieve a uniform and efficient distribution of a substance within the target. In this study it was demonstrated, both numerically and experimentally, how an ultrasonically actuated med-

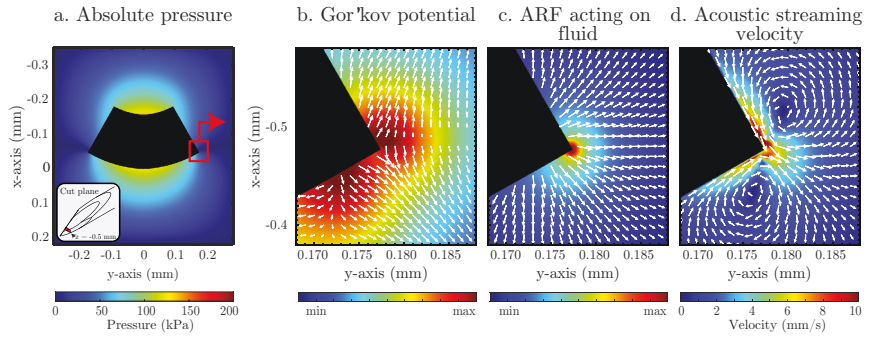


**Figure 4.4.** Representation of some relevant acoustic variables evaluated on a cross-sectional plane located at  $z = -0.5$  mm from the needle tip. **(a)** Shows the absolute pressure field radiated from the needle boundary, while **(b)** represents the Gor'kov potential, which denotes the level of attraction of the nanoparticles within the acoustic field and **(c)** represents the ARF acting on the liquid, which gives rise to **(d)** the streaming patterns. In Publication II it was demonstrated that the ARF acting on the liquid is two orders of magnitude greater compared to the force acting on the nanoparticles alone, revealing that the latter brings a negligible contribution to the acceleration of nanoparticles. The results also show that the streaming is highly localized at the sharp-edges of the needle geometry **(d)**, resembling the so called sharp-edge streaming reported in literature.

ical needle can increase the volume of an agarose gel diffused by the tracer, when the needle was actuated for 10 min at a TAP of 20 mW. The numerical results provide evidence on how the same concept can increase up to three times the volume of liver tissue exposed by the tracer, when the needle is actuated for 10 s at a TAP of 20 mW under an applied flow rate of  $10 \mu\text{L min}^{-1}$ , as compared to when no US was employed. This technology could be a minimally-invasive and low-cost alternative to expensive ultrasonic clinical methods, such as magnetic imaging-guided high-intensity focused ultrasound (HIFU), used for image-guided delivery of drugs into a target location.

### 4.3 Publication III

Publication III demonstrated how an ultrasonically actuated needle can be used to generate cavitation events in soft tissue. Numerically, the extent of cavitation activity was first studied, when the needle was excited at the frequency of 33 kHz and at different TAP levels. Experimentally, a method for visualizing the needle movement inside a shallow portion of *ex vivo* bovine liver was developed. This method involved using HS imaging in combination with a collimated beam of light generated by a

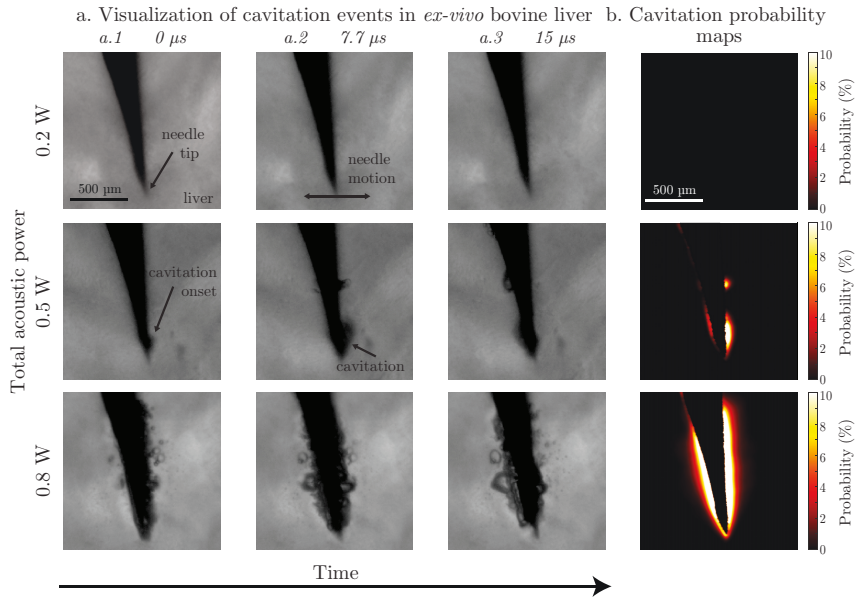


**Figure 4.5.** (a) Exemplary HS video frames showing cavitation events taking place at the needle tip at 3 different TAP levels. (b) The probability maps, which show the probability of each pixel belonging to an optical projection of a cavitation bubble, demonstrate that no cavitation activity is recorded at 0.2 W, while it is more frequent at higher TAP levels. These results show how cavitation can be generated on-demand and in a localized manner near the needle tip.

halogen fiber optic illuminator, which permitted to record back-lit footages of the cavitation activity induced by the needle action inside tissue (Figure 4.5). The main finding in both numerical and experimental data was that cavitation mostly took place and the needle tip, exhibiting elevated activity at 0.5 W TAP and above, while no cavitation took place at TAP = 0.2 W. Furthermore, the study includes a range of *in silico* investigations broadening the understanding of cavitation dynamics near the needle tip. The results presented in Publication III are interesting because, to our knowledge, this study is the first one to prove that acoustic cavitation inside tissue can be created with hypodermic needles with high localization at the needle tip. Therefore, this study is expected to open up an avenue to develop novel minimally invasive interventions by employing thin needles and localized micro-bubble activity, such as bubble-activated drug and gene delivery, US-enhanced fine-needle biopsy and fractionation of small tumors or calculi.

## 5. Discussion

In this Thesis, it was investigated how non-linear ultrasonics can be used to functionalize the tip of a medical needle. NLU phenomena associated with the emission of sound from the needle tip were characterized with specific focus on cavitation, acoustic radiation pressure, acoustic streaming and atomization. These effects took place within a volume that was defined as SonoLancet. In this approach, the conventional hypodermic needle structure employs the lumen as a conduit to guide sound energy to the needle tip, wherein the US action is amplified due to the converging shape of its bevel. The resulting sound emission from the needle tip has a high enough intensity to produce non-linear effects at the tip of the needle, within the SonoLancet. Limiting the US action to the proximity of the needle tip provides spatio-temporal control of sound-tissue interaction.

The numerical and experimental results demonstrated that cavitation can be made to take place locally at the tip of the needle (Publications I and III). In fact, since inertial cavitation is a threshold phenomenon, cavitation is more likely to appear at the needle tip location, where the acoustic energy is concentrated (Publications I and III). Moreover, cavitation activity can be easily controlled, as the strength of it is dependent on the delivered TAP (Publication III). Overall, the ability to generate cavitation at will with spatial control could enable its use in applications such as tumor ablation [104], permeation of tissue matrix for enhanced stem cell delivery or migration, bubble-enhanced poration of cells and sonoporation [105, 106]. Moreover, the observed cavitation events could potentially lead to shockwave formation, as widely known and reported in literature [81, 82, 107]. Generation of shockwaves and associated shear forces, arising from imploding cavitation bubbles [108], could find use in applications such as lithotripsy [56] or controlled softening of calcified vessels [109] with mechanical stress gradients [110].

The acoustic streaming, caused by localized US emission from the needle tip (Publications I and II), can be used to enhance the convection of the fluid phase inside a porous matrix (Publication II), thus being a major contributor to the fluid and nanoparticle transport mechanisms in porous media. The unidirectional motion of fluids could enhance pharmaceutical effectiveness [111] and facilitate the delivery of drugs or nanoparticles to tissues with compromised perfusion [112]. The advantage of employing a hypodermic needle as a waveguide to deliver the acoustic energy to the target is that acoustic streaming can be generated to treat lesions within anatomical regions, such as in the lungs or in the liver, that would be difficult to reach with conventional HIFU based systems. The complication arising from using HIFU to treat lesions within the thoracic region or in the hepatic dome, for example, is mainly associated with the acoustic shadowing of bones and gas, which can hinder the formation of a proper US focus at the target [113, 114]. By using an ultrasonic needle for the local administration of drugs, not only these anatomical structures could be easily bypassed, but also one could avoid side effects and complications associated with other commonly used routes of drug administration (*e.g.*, intravenous injection, systemic administration) [115, 116, 117, 118] and minimize side bioeffects [114, 119] along the beam path that one could observe in HIU applications.

The ultrasonically actuated medical needle enables atomization of small volumes of liquid (Publication I). The current arrangement allows one to transform liquid into micro-droplets with control over the size of the ejected droplets, importantly directivity of the droplet jets (Publication I). The needle structure can facilitate several eigenfrequencies. The operation frequency can be easily changed across eigenfrequencies, allowing one to also change size distribution of the generated microdroplets (Publication I). This feature would make the ultrasonic needle a versatile tool to atomize liquids if compared to common US atomizers, which typically operate at a fixed frequency [120, 121, 122], and could be exploited to spread substances over a small surface, or to deliver drugs in small bodily cavities such as those present in the upper respiratory system. Moreover, since the size distribution of the atomised droplets can be easily changed by shifting the operating frequency, one would enable deposition of drugs at a prescribed depth in the respiratory system, being the droplet deposition efficiency along the respiratory tract dependent on the droplet diameter

Perhaps most importantly, the Thesis provided evidence to the capability

of an ultrasonically actuated medical needle to add value to the biopsy applications (Publication I). The results showed that, when the hypodermic needle is made to oscillate at the frequency of  $\sim 33$  kHz, the mass of the sample obtained from soft tissues can be systematically increased up to  $3\text{-}6\times$  on average, as compared to the yield obtained with a state-of-the-art FNAB procedure. The mechanism behind the improved tissue yield might be that the mechanical forces arising from shear and the herein described NLU phenomena synergically contribute towards the detachment of cells and tissue construct from the surrounding tissue. However, based on the results presented in Publication III, at low TAP levels ( $\leq 0.2$  W), these NLU effects, namely cavitation, acoustic streaming and ARF, are expected to have a negligible influence in tissue.

The tissue cutting mechanism of conventional FNAB can be explained by the interpretation provided by Kreula *et al.* [123], which suggests that the sample yield enhancement is a result of the combined action between the suction force, provided by the syringe, and the operator's hand movement. The suction is in fact needed to draw the detached cells and tissue into the needle, while the hand movement is essential to slice off the portion of tissue that has bulged into the needle opening. In this regard, the ultrasonic actuation of the needle introduces an additional flexural component of the needle movement that can help in facilitating the cutting process by allowing small regions of tissue to be loaded with forces exceeding the yield point and, thereby, contributing to yield enhancement.

At higher TAP levels ( $>0.2$  W) the NLU phenomena are anticipated to have an effect on tissue proportionally dependent on the delivered TAP. High strain rates can be generated at the oscillating boundary of gas/tissue interface [124, 125] and shear stresses, arising from velocity gradients generated by acoustic streaming, can be also produced in this context [112]. These could potentially contribute to influence the viscoelastic mechanical properties of soft tissue [126] that might facilitate the tissue cutting mechanisms, resulting in the systematic improvement of tissue yield that was observed when increasing TAP from  $0.5$  W to  $0.8$  W. These findings are expected to be of great importance especially in cancer diagnostics, in particular to FNAB applications, which suffers from insufficient tissue yield in up to 34% of histopathological and 50% of molecular diagnostic assessments [13, 12]. In fact, USEFNAB enhances the volume of the collected sample; therefore, it is expected to contribute towards a higher probability to capture pathological cells. However, employing higher TAP

levels (*e.g.*  $> 0.8\text{ W}$ ) could elevate the probability of inducing cavitation related bioeffects and tissue damage, which might compromise the quality of the biopsy sample. For this reason, a trade-off between the employed TAP and cell integrity has to be accurately defined in future studies in order to maximize the tissue yield for diagnostic needs, while minimizing the sample-quality-to-quantity ratio (Publication I). While representing a limitation in terms of maximum TAP level applicable for biopsy applications, this aspect can be turned into a therapeutic advantage, for example, for the treatment of tumors by means of pathological destruction of tissue, which has been extensively discussed in Publication III.

By bringing precisely controlled US energy to a specific location, it is foreseen that the SonoLancet has the potential to add value to several medical applications such as tissue biopsy, drug and gene delivery or surgical procedures in a portable and cost-effective manner.

## 6. Conclusion

In this Thesis, it was shown that non-linear ultrasonics can be used to potentially convert a standard hypodermic needle into a versatile medical instrument, able to cover a multitude of medical functions. To conclude:

1. A method enabling powerful dipole-like acoustic emission from the needle tip, which can exhibit NLU phenomena in a confined volume, was demonstrated. This activated volume, which is defined as the SonoLancet, is capable of influencing matter beyond the functions of a conventional medical needle (Publication I). Specifically, NLU phenomena were demonstrated and quantified on micro- to millimetre scale. These phenomena included directional translation of microparticles and liquid, both in a free liquid and in agarose gels (Publications I and II), controlled generation of airborne microdroplets (Publication I) and the capability to generate cavitation activity in different media, including water, ballistic gelatin and soft tissue (Publications I and III).
2. The numerical results confirmed the hypothesis that the ultrasonic energy is highly localized at the tip of the needle. As a consequence, it was found out that strong streamings of fluid, emanating from the sharp edges of the needle tip, can be generated to translate nanoparticles and fluids in porous media (Publication II). Moreover, the simulation results indicated that, when the needle is actuated in soft tissue, cavitation activity mostly takes place in the vicinity of the tip of the needle, which was also confirmed experimentally (Publication III).
3. This technology could potentially contribute to a number of medical applications. For example, the SonoLancet interactions with tissue were exemplified in the FNAB application, and the advantages of improving

the sample yield were discussed (Publication I). Drug and gene delivery applications that could benefit from this concept have been also elaborated (Publications II and III), as well as applications aiming at controlled tissue disruption, such as histotripsy or lithotripsy (Publication III).

This study is the first report to quantify and describe the NLU phenomena associated with ultrasonically actuated medical needles. The concept of SonoLancet, which has the potential to lead to a radical transformation of medical needles into spatially and temporally controlled medical instruments, was defined and demonstrated. SonoLancet has the potential to give conventional medical needles enhanced new functions in many medical applications, such as tissue biopsy, molecular diagnostics, drug or gene delivery, cell modulation, and minimally invasive surgical procedures.

# References

- [1] L. J. Bliquez and E. J. Munro, "Paulakion and securicella: Two Hitherto unidentified Greco-Roman veterinary instruments," *Mnemosyne*, vol. 60, no. 3, pp. 490–494, 2007.
- [2] W. R. Bett, "The History and Conquest of Common Diseases," *Southern Medical Journal*, vol. 48, no. 5, p. 558, 1955.
- [3] A. M. Hauri, G. L. Armstrong, and Y. J. Hutin, "The global burden of disease attributable to contaminated injections given in health care settings," *International Journal of STD and AIDS*, vol. 15, no. 1, pp. 7–16, 2004.
- [4] T. Kucklick, "Introduction to needles and cannulae," in *The Medical Device R and D Handbook*, ch. 5, pp. 89–112, FL, USA: CRC Press, 2005.
- [5] J. G. Hamilton, "Needle phobia: A neglected diagnosis," *Journal of Family Practice*, vol. 41, no. 2, pp. 169–175, 1995.
- [6] K. Jenkins, "Needle phobia: A psychological perspective," *British Journal of Anaesthesia*, vol. 113, pp. 4–6, 7 2014.
- [7] V. del Barrio, "Diagnostic and Statistical Manual of Mental Disorders," in *Encyclopedia of Applied Psychology, Three-Volume Set*, pp. 607–614, 2004.
- [8] E. S. Ayala, A. E. Meuret, and T. Ritz, "Treatments for blood-injury-injection phobia: A critical review of current evidence," *Journal of Psychiatric Research*, vol. 43, no. 15, pp. 1235–1242, 2009.
- [9] H. Y. Ji, E. K. Kim, J. K. Min, Y. L. Ji, and K. O. Ki, "Missed breast cancers at us-guided core needle biopsy: How to reduce them," *Radiographics*, vol. 27, no. 1, pp. 79–94, 2007.
- [10] K. P. Pritzker and H. J. Nieminen, "Needle biopsy adequacy in the era of precision medicine and value-based health care," *Archives of Pathology and Laboratory Medicine*, vol. 143, no. 11, pp. 1399–1415, 2019.
- [11] M. E. Gutierrez, K. Choi, R. B. Lanman, E. J. Licitra, S. M. Skrzypczak, R. Pe Benito, T. Wu, S. Arunajadai, S. Kaur, H. Harper, A. L. Pecora, E. V. Schultz, and S. L. Goldberg, "Genomic Profiling of Advanced Non-Small Cell Lung Cancer in Community Settings: Gaps and Opportunities," *Clinical Lung Cancer*, vol. 18, pp. 651–659, 11 2017.
- [12] A. Nassar, "Core needle biopsy versus fine needle aspiration biopsy in breast-A historical perspective and opportunities in the modern era," *Diagnostic Cytopathology*, vol. 39, pp. 380–388, 5 2011.

- [13] H. J. Carson, G. A. Saint Martin, M. J. Castelli, and P. Gattuso, "Unsatisfactory aspirates from fine-needle aspiration biopsies: A review," *Diagnostic Cytopathology*, vol. 12, pp. 280–284, 5 1995.
- [14] L. Gui, R. Xiao, X. Liao, Y. Kuang, M. Sadiq, Z. Chunnian, S. Cochran, and Z. Huang, "Automatic frequency tracking system for needle actuating device," in *IEEE International Ultrasonics Symposium, IUS*, (IL, USA), pp. 815–818, 9 2014.
- [15] Y. Kuang, A. Hilgers, M. Sadiq, S. Cochran, G. Corner, and Z. Huang, "Modelling and characterisation of a ultrasound-actuated needle for improved visibility in ultrasound-guided regional anaesthesia and tissue biopsy," *Ultrasonics*, vol. 69, pp. 38–46, 7 2016.
- [16] M. R. Sadiq, S. Cochran, X. Liao, and Z. Huang, "Enhanced US-guided needle intervention through ultrasound actuation of a standard needle," *IEEE International Ultrasonics Symposium, IUS*, vol. 4, pp. 827–830, 2014.
- [17] X. Liao, M. Sadiq, Y. Kuang, G. Corner, S. Cochran, and Z. Huang, "Performance optimization of ultrasonic needle actuating device for insertion operation into tissue mimics," in *IEEE International Ultrasonics Symposium, IUS*, (IL, USA), pp. 823–826, IEEE, 9 2014.
- [18] X. Liao, M. Sadiq, G. Corner, S. Cochran, and Z. Huang, "Reduced penetration force through ultrasound activation of a standard needle: An experimental and computational study," in *IEEE International Ultrasonics Symposium, IUS*, vol. 1, (Prague, Czech Republic), pp. 1436–1439, 7 2013.
- [19] K. Yanagida, H. Katayose, H. Yazawa, Y. Kimura, K. Konnai, and A. Sato, "The usefulness of a piezo-micromanipulator in intracytoplasmic sperm injection in humans," *Human Reproduction*, vol. 14, no. 2, pp. 448–453, 1999.
- [20] M. Muthaiyan Shanmugam and H. Manoj, "Microinjection for Single-Cell Analysis and Therapy," in *Handbook of Single Cell Technologies*, pp. 1–27, Springer Singapore, 2021.
- [21] W. Johnson, C. Dai, J. Liu, X. Wang, D. K. Luu, Z. Zhang, C. Ru, C. Zhou, M. Tan, H. Pu, S. Xie, Y. Peng, J. Luo, and Y. Sun, "A Flexure-Guided Piezo Drill for Penetrating the Zona Pellucida of Mammalian Oocytes," *IEEE Transactions on Biomedical Engineering*, vol. 65, no. 3, pp. 678–686, 2018.
- [22] H. Katayose, K. Yanagida, T. Shinoki, T. Kawahara, T. Horiuchi, and A. Sato, "Efficient injection of bull spermatozoa into oocytes using a Piezo-driven pipette," *Theriogenology*, vol. 52, pp. 1215–1224, 11 1999.
- [23] S. Takeuchi, H. Minoura, T. Shibahara, X. Shen, N. Futamura, and N. Toyoda, "Comparison of piezo-assisted micromanipulation with conventional micromanipulation for intracytoplasmic sperm injection into human oocytes," *Gynecologic and Obstetric Investigation*, vol. 52, no. 3, pp. 158–162, 2001.
- [24] Y. Kimura and R. Yanagimachi, "Intracytoplasmic sperm injection in the mouse," *Biology of Reproduction*, vol. 52, pp. 709–720, 4 1995.

- [25] I. M. Bahadur, C. Y. Wong, X. Jiang, and J. K. Mills, "Dynamic modelling and embryo zona pellucida perforation experiments with piezoelectric actuated micro-needles," in *2017 IEEE International Conference on Mechatronics and Automation, ICMA 2017*, pp. 445–450, Institute of Electrical and Electronics Engineers Inc., 8 2017.
- [26] I. M. Bahadur, C. Y. Wong, X. Jiang, and J. K. Mills, "Dynamic modelling, simulation and experiments of a micro-cutter with applications to cell perforation," *International Journal of Mechatronics and Automation*, vol. 8, no. 1, pp. 22–33, 2021.
- [27] T. Wu, Z. Zhou, Q. Wang, X. Yang, and M. Xiao, "A Miniature Probe for Ultrasonic Penetration of a Single Cell," *Sensors*, vol. 9, pp. 3325–3336, 5 2009.
- [28] Z. Zhou, M. Xiao, X. Yang, and T. Wu, "A single cell penetration system by ultrasonic driving," in *2008 International Conference on Optical Instruments and Technology: MEMS/NEMS Technology and Applications*, vol. 7159, p. 715907, 2008.
- [29] C. H. Lee and A. Lal, "Single microdroplet ejection using an ultrasonic longitudinal mode with a PZT/tapered glass capillary," *IEEE Transactions on Ultrasonics, Ferroelectrics, and Frequency Control*, vol. 51, pp. 1514–1522, 11 2004.
- [30] J. S. Bach and H. Bruus, *Theory of acoustic trapping of microparticles in capillary tubes*, vol. 101. American Physical Society, 2 2020.
- [31] M. K. Araz, C. H. Lee, and A. Lal, "Ultrasonic separation in microfluidic capillaries," *Proceedings of the IEEE Ultrasonics Symposium*, vol. 2, pp. 1111–1114, 2003.
- [32] I. Gralinski, T. Alan, and A. Neild, "Non-contact acoustic trapping in circular cross-section glass capillaries: A numerical study," *The Journal of the Acoustical Society of America*, vol. 132, p. 2978, 11 2012.
- [33] D. N. Armstrong, W. L. Ambroze, M. E. Schertzer, and G. R. Orangio, "Harmonic Scalpel® vs. electrocautery hemorrhoidectomy: A prospective evaluation," *Diseases of the Colon and Rectum*, vol. 44, no. 4, pp. 558–564, 2001.
- [34] K. Ebina, H. Hasegawa, and H. Kanai, "Investigation of frequency characteristics in cutting of soft tissue using prototype ultrasonic knives," *Japanese Journal of Applied Physics, Part 1: Regular Papers and Short Notes and Review Papers*, vol. 46, pp. 4793–4800, 7 2007.
- [35] Y. Tsuda, E. Mori, and S. Ueha, "Experimental Study of Ultrasonic Surgical Knife," *Japanese Journal of Applied Physics*, vol. 22, p. 105, 1 1983.
- [36] D. Ensminger and L. J. Bond, *Ultrasonics: Fundamentals, technologies, and applications, third edition*. CRC press, 2011.
- [37] A. D. Walmsley, "Applications of ultrasound in dentistry," *Ultrasound in Medicine and Biology*, vol. 14, pp. 7–14, 1 1988.
- [38] J. E. Kennedy, "High-intensity focused ultrasound in the treatment of solid tumours," *Nature Reviews Cancer*, vol. 5, pp. 321–327, 4 2005.

- [39] L. Zhang and Z. B. Wang, "High-intensity focused ultrasound tumor ablation: Review of ten years of clinical experience," *Frontiers of Medicine in China*, vol. 4, pp. 294–302, 8 2010.
- [40] Y.-F. Zhou, "High intensity focused ultrasound in clinical tumor ablation," *World Journal of Clinical Oncology*, vol. 2, no. 1, p. 8, 2011.
- [41] N. Sheikov, N. McDannold, N. Vykhodtseva, F. Jolesz, and K. Hynynen, "Cellular mechanisms of the blood-brain barrier opening induced by ultrasound in presence of microbubbles," *Ultrasound in Medicine and Biology*, vol. 30, no. 7, pp. 979–989, 2004.
- [42] S. Meairs and A. Alonso, "Ultrasound, microbubbles and the blood-brain barrier," *Progress in Biophysics and Molecular Biology*, vol. 93, pp. 354–362, 1 2007.
- [43] E. E. Konofagou, Y.-S. Tunga, J. Choia, T. Deffieux, B. Baseria, and F. Vlachosa, "Ultrasound-Induced Blood-Brain Barrier Opening," *Current Pharmaceutical Biotechnology*, vol. 13, pp. 1332–1345, 6 2012.
- [44] S. Hernot and A. L. Klibanov, "Microbubbles in ultrasound-triggered drug and gene delivery," *Advanced Drug Delivery Reviews*, vol. 60, pp. 1153–1166, 6 2008.
- [45] J. Castle, M. Butts, A. Healey, K. Kent, M. Marino, and S. B. Feinstein, "Ultrasound-mediated targeted drug delivery: Recent success and remaining challenges," *American Journal of Physiology - Heart and Circulatory Physiology*, vol. 304, pp. H350–H357, 2 2013.
- [46] H. Chen and J. H. Hwang, "Ultrasound-targeted microbubble destruction for chemotherapeutic drug delivery to solid tumors," *Journal of Therapeutic Ultrasound*, vol. 1, p. 10, 7 2013.
- [47] A. L. Papa, N. Korin, M. Kanapathipillai, A. Mammoto, T. Mammoto, A. Jiang, R. Mannix, O. Uzun, C. Johnson, D. Bhatta, G. Cuneo, and D. E. Ingber, "Ultrasound-sensitive nanoparticle aggregates for targeted drug delivery," *Biomaterials*, vol. 139, pp. 187–194, 9 2017.
- [48] T. Ikeda, S. Yoshizawa, M. Tosaki, J. S. Allen, S. Takagi, N. Ohta, T. Kitamura, and Y. Matsumoto, "Cloud cavitation control for lithotripsy using high intensity focused ultrasound," *Ultrasound in Medicine and Biology*, vol. 32, pp. 1383–1397, 9 2006.
- [49] A. D. Maxwell, C. A. Cain, A. P. Duryea, L. Yuan, H. S. Gurm, and Z. Xu, "Noninvasive Thrombolysis Using Pulsed Ultrasound Cavitation Therapy - Histotripsy," *Ultrasound in Medicine and Biology*, vol. 35, pp. 1982–1994, 12 2009.
- [50] D. Bommannan, H. Okuyama, P. Stauffer, and R. H. Guy, "Sonophoresis. I. The Use of High-Frequency Ultrasound to Enhance Transdermal Drug Delivery," *Pharmaceutical Research: An Official Journal of the American Association of Pharmaceutical Scientists*, vol. 9, no. 4, pp. 559–564, 1992.
- [51] I. Lentacker, I. De Cock, R. Deckers, S. C. De Smedt, and C. T. Moonen, "Understanding ultrasound induced sonoporation: Definitions and underlying mechanisms," *Advanced Drug Delivery Reviews*, vol. 72, pp. 49–64, 2014.

- [52] G. U. Dachs, G. J. Dougherty, I. J. Stratford, and D. J. Chaplin, "Targeting gene therapy to cancer: A review," *Oncology Research*, vol. 9, no. 6-7, pp. 313–325, 1997.
- [53] M. Aryal, C. D. Arvanitis, P. M. Alexander, and N. McDannold, "Ultrasound-mediated blood-brain barrier disruption for targeted drug delivery in the central nervous system," *Advanced Drug Delivery Reviews*, vol. 72, pp. 94–109, 6 2014.
- [54] J. Gehl, "Electroporation: Theory and methods, perspectives for drug delivery, gene therapy and research," *Acta Physiologica Scandinavica*, vol. 177, pp. 437–447, 4 2003.
- [55] W. W. Roberts, T. L. Hall, K. Ives, J. S. Wolf, J. B. Fowlkes, and C. A. Cain, "Pulsed cavitation ultrasound: A noninvasive technology for controlled tissue ablation (histotripsy) in the rabbit kidney," *Journal of Urology*, vol. 175, pp. 734–738, 2 2006.
- [56] S. Yoshizawa, T. Ikeda, A. Ito, R. Ota, S. Takagi, and Y. Matsumoto, "High intensity focused ultrasound lithotripsy with cavitating microbubbles," *Medical and Biological Engineering and Computing*, vol. 47, pp. 851–860, 4 2009.
- [57] J. S. Patton and P. R. Byron, "Inhaling medicines: Delivering drugs to the body through the lungs," *Nature Reviews Drug Discovery*, vol. 6, pp. 67–74, 1 2007.
- [58] I. A. Viktorov, *Rayleigh and Lamb Waves*. Plenum Press, 1967.
- [59] K. Y. Jhang, "Nonlinear ultrasonic techniques for non-destructive assessment of micro damage in material: A Review," *International Journal of Precision Engineering and Manufacturing*, vol. 10, no. 1, pp. 123–135, 2009.
- [60] L. Kinsler, A. Frey, A. Coppens, and J. Sanders, *Fundamentals of Acoustics (4th Edition)*. Wiley, 1999.
- [61] C. J. Montrose, "Sound and Matter: Ultrasonic Absorption . An Introduction to the Theory of Sound Absorption and Dispersion in Gases, Liquids, and Solids.," *Science*, vol. 158, pp. 1441–1441, 12 1967.
- [62] W. P. Mason, "Physical Acoustics and the Properties of Solids," *The Journal of the Acoustical Society of America*, vol. 28, no. 6, pp. 1197–1206, 1956.
- [63] A. J. Matheson, "Chapter 3. Molecular acoustics," in *Annual Reports on the Progress of Chemistry, Section A: General Physical and Inorganic Chemistry*, vol. 68, ch. Chapter 3, pp. 27–45, The Royal Society of Chemistry, 1 1971.
- [64] M. W. Urban, A. Alizad, W. Aquino, J. F. Greenleaf, and M. Fatemi, "A Review of Vibro-acoustography and its Applications in Medicine," *Current Medical Imaging Reviews*, vol. 7, pp. 350–359, 11 2011.
- [65] P. J. Westervelt, "The Theory of Steady Forces Caused by Sound Waves," *The Journal of the Acoustical Society of America*, vol. 23, pp. 312–315, 6 1951.
- [66] W. L. M. Nyborg, "Acoustic Streaming," *Physical Acoustics*, vol. 2, pp. 265–331, 1965.

- [67] D. Bermúdez-aguirre, T. Mobbs, and G. V. Barbosa-cánovas, *Ultrasound Technologies for Food and Bioprocessing*. Food Engineering Series, New York, NY: Springer New York, 2011.
- [68] N. Riley, "Oscillating viscous flows," *Mathematika*, vol. 12, no. 2, pp. 161–175, 1965.
- [69] N. Riley, "Steady streaming," *Annual Review of Fluid Mechanics*, vol. 33, pp. 43–65, 1 2001.
- [70] M. Wiklund, R. Green, and M. Ohlin, "Acoustofluidics 14: Applications of acoustic streaming in microfluidic devices," *Lab on a Chip*, vol. 12, pp. 2438–2451, 7 2012.
- [71] J. W. Strutt, "On the Circulation of Air observed in Kundt's Tubes, and on some Allied Acoustical Problems," *Scientific Papers*, vol. 175, pp. 239–257, 2011.
- [72] C. K. Holland and R. E. Apfel, "Thresholds for transient cavitation produced by pulsed ultrasound in a controlled nuclei environment," *The Journal of the Acoustical Society of America*, vol. 88, no. 5, pp. 2059–2069, 1990.
- [73] T. G. Leighton and R. E. Apfel, "The Acoustic Bubble," *The Journal of the Acoustical Society of America*, 1994.
- [74] F. R. Young, *Cavitation*. World Scientific Publishing Company, 11 1999.
- [75] K. Yasui, T. Tuziuti, J. Lee, T. Kozuka, A. Towata, and Y. Iida, "The range of ambient radius for an active bubble in sonoluminescence and sonochemical reactions," *Journal of Chemical Physics*, vol. 128, no. 18, p. 184705, 2008.
- [76] A. A. Atchley, "The blake threshold of a cavitation nucleus having a radius-dependent surface tension," *The Journal of the Acoustical Society of America*, vol. 85, pp. 152–157, 6 1989.
- [77] N. Takahashi, S. Ohtori, T. Saisu, H. Moriya, and Y. Wada, "Second application of low-energy shock waves has a cumulative effect on free nerve endings," *Clinical Orthopaedics and Related Research*, vol. 443, pp. 315–319, 2006.
- [78] W. Lauterborn, T. Kurz, and I. Akhatov, "Nonlinear Acoustics in Fluids," in *Springer Handbooks*, pp. 257–297, Springer, 2007.
- [79] R. T. Beyer, "Nonlinear Acoustics," in *Physical Acoustics*, vol. 2, pp. 231–264, Academic Press, 1 1965.
- [80] L. Bjørnø, "Introduction to nonlinear acoustics," in *Physics Procedia*, vol. 3, pp. 5–16, Elsevier, 1 2010.
- [81] V. Minsier and J. Proost, "Shock wave emission upon spherical bubble collapse during cavitation-induced megasonic surface cleaning," *Ultrasonics Sonochemistry*, vol. 15, no. 4, pp. 598–604, 2008.
- [82] E. A. Brujan, T. Ikeda, and Y. Matsumoto, "Jet formation and shock wave emission during collapse of ultrasound-induced cavitation bubbles and their role in the therapeutic applications of high-intensity focused ultrasound," *Physics in Medicine and Biology*, vol. 50, no. 20, pp. 4797–4809, 2005.

- [83] N. Kong, D. S. Ha, A. Erturk, and D. J. Inman, “Resistive impedance matching circuit for piezoelectric energy harvesting,” *Journal of Intelligent Material Systems and Structures*, vol. 21, pp. 1293–1302, 9 2010.
- [84] Mathworks, “MATLAB.” Available at: [www.mathworks.com](http://www.mathworks.com), 2016.
- [85] “COMSOL Multiphysics.” Available at [www.comsol.com](http://www.comsol.com), 2014.
- [86] M. Guizar-Sicairos, S. T. Thurman, and J. R. Fienup, “Efficient subpixel image registration algorithms,” *Optics Letters*, vol. 33, no. 2, p. 156, 2008.
- [87] K. Jambunathan, X. Y. Ju, B. N. Dobbins, and S. Ashforth-Frost, “An improved cross correlation technique for particle image velocimetry,” *Measurement Science and Technology*, vol. 6, no. 5, pp. 507–514, 1995.
- [88] P. Movahed, W. Kreider, A. D. Maxwell, S. B. Hutchens, and J. B. Freund, “Cavitation-induced damage of soft materials by focused ultrasound bursts: A fracture-based bubble dynamics model,” *The Journal of the Acoustical Society of America*, vol. 140, pp. 1374–1386, 8 2016.
- [89] Y. Wang, R. K. Chen, B. L. Tai, P. W. McLaughlin, and A. J. Shih, “Optimal needle design for minimal insertion force and bevel length,” *Medical Engineering and Physics*, vol. 36, pp. 1093–1100, 9 2014.
- [90] M. Sadiq, *Enhanced Biopsy and Regional Anaesthesia through Ultrasound Actuation of a Standard Needle*. PhD thesis, University of Dundee, 2013.
- [91] I. Sharma, “Continuum Mechanics,” in *Shapes and Dynamics of Granular Minor Planets*, pp. 15–49, Springer, 2017.
- [92] J. D. N. Cheeke, *Fundamentals and applications of ultrasonic waves, second edition*. CRC Press, 2017.
- [93] M. A. Solovchuk, T. W. Sheu, M. Thiriet, and W. L. Lin, “On a computational study for investigating acoustic streaming and heating during focused ultrasound ablation of liver tumor,” *Applied Thermal Engineering*, vol. 56, pp. 62–76, 7 2013.
- [94] R. T. Beyer, “Nonlinear Acoustics,” in *Comprehensive Biomedical Physics*, vol. 2, pp. 231–264, Elsevier B.V., 1965.
- [95] S. J. Lighthill, “Acoustic streaming,” *Journal of Sound and Vibration*, vol. 61, no. 3, pp. 391–418, 1978.
- [96] J. B. Keller and M. Miksis, “Bubble oscillations of large amplitude,” *The Journal of the Acoustical Society of America*, vol. 68, no. 2, pp. 628–633, 1980.
- [97] D. elipe Gaitan, L. A. Crum, C. C. Church, and R. A. Roy, “Sonoluminescence and bubble dynamics for a single, stable, cavitation bubble,” *The Journal of the Acoustical Society of America*, vol. 91, no. 6, pp. 3166–3183, 1992.
- [98] T. L. Hall, L. J. Layfield, A. Philippe, and D. L. Rosenthal, “Sources of diagnostic error in fine needle aspiration of the thyroid,” *Cancer*, vol. 63, no. 4, pp. 718–725, 1989.
- [99] N. P. Caraway, N. Sneige, and N. A. Samaan, “Diagnostic pitfalls in thyroid fine-needle aspiration: A review of 394 cases,” *Diagnostic Cytopathology*, vol. 9, no. 3, pp. 345–350, 1993.

- [100] Z. W. Baloch, S. Fleisher, V. A. LiVolsi, and P. K. Gupta, "Diagnosis of "follicular neoplasm": A gray zone in thyroid fine-needle aspiration cytology," *Diagnostic Cytopathology*, vol. 26, no. 1, pp. 41–44, 2002.
- [101] M. Ovchinnikov, J. Zhou, and S. Yalamanchili, "Acoustic streaming of a sharp edge," *The Journal of the Acoustical Society of America*, vol. 136, pp. 22–29, 7 2014.
- [102] C. Zhang, X. Guo, L. Royon, and P. Brunet, "Acoustic streaming generated by sharp edges: The coupled influences of liquid viscosity and acoustic frequency," *Micromachines*, vol. 11, pp. 1–15, 6 2020.
- [103] P. H. Huang, N. Nama, Z. Mao, P. Li, J. Rufo, Y. Chen, Y. Xie, C. H. Wei, L. Wang, and T. J. Huang, "A reliable and programmable acoustofluidic pump powered by oscillating sharp-edge structures," *Lab on a Chip*, vol. 14, pp. 4319–4323, 10 2014.
- [104] Y. Zhou, "High intensity focused ultrasound in clinical tumor ablation," *World Journal of Clinical Oncology*, vol. 2, no. 1, p. 8, 2011.
- [105] S. Mehier-Humbert, T. Bettinger, F. Yan, and R. H. Guy, "Plasma membrane poration induced by ultrasound exposure: Implication for drug delivery," *Journal of Controlled Release*, vol. 104, no. 1, pp. 213–222, 2005.
- [106] S. Hernot and A. L. Klibanov, "Microbubbles in ultrasound-triggered drug and gene delivery," *Advanced Drug Delivery Reviews*, vol. 60, pp. 1153–1166, 6 2008.
- [107] T. Leong, M. Ashokkumar, and S. Kentish, "The growth of bubbles in an acoustic field by rectified diffusion," in *Handbook of Ultrasonics and Sonochemistry*, pp. 69–98, 2016.
- [108] I. Akhatov, O. Lindau, A. Topolnikov, R. Mettin, N. Vakhitova, and W. Lauterborn, "Collapse and rebound of a laser-induced cavitation bubble," *Physics of Fluids*, vol. 13, no. 10, pp. 2805–2819, 2001.
- [109] R. J. Siegel, M. C. Fishbein, J. Forrester, K. Moore, E. DeCastro, L. Daykhovskiy, and T. A. DonMichael, "Ultrasonic plaque ablation: A new method for recanalization of partially or totally occluded arteries," *Circulation*, vol. 78, no. 6, pp. 1443–1448, 1988.
- [110] M. R. Bailey, V. A. Khokhlova, O. A. Sapozhnikov, S. G. Kargl, and L. A. Crum, "Physical mechanisms of the therapeutic effect of ultrasound (a review)," *Acoustical Physics*, vol. 49, pp. 369–388, 7 2003.
- [111] S. Mitragotri, "Healing sound: The use of ultrasound in drug delivery and other therapeutic applications," *Nature Reviews Drug Discovery*, vol. 4, no. 3, pp. 255–260, 2005.
- [112] J. Wu, "Acoustic streaming and its applications," *Fluids*, vol. 3, p. 108, 12 2018.
- [113] Y. S. Kim, H. Rhim, J. C. Min, K. L. Hyo, and D. Choi, "High-intensity focused ultrasound therapy: An overview for radiologists," *Korean Journal of Radiology*, vol. 9, pp. 291–302, 8 2008.

- [114] Y. Long, Q. Zeng, X. He, H. Ye, Y. Su, R. Zheng, J. Yu, E. Xu, and K. Li, "One-lung ventilation for percutaneous thermal ablation of liver tumors in the hepatic dome," *International Journal of Hyperthermia*, vol. 37, pp. 49–54, 1 2020.
- [115] J. Truong, A. T. Yan, G. Cramarossa, and K. K. Chan, "Chemotherapy-induced cardiotoxicity: Detection, prevention, and management," *Canadian Journal of Cardiology*, vol. 30, pp. 869–878, 8 2014.
- [116] K. Bergkvist and Y. Wengström, "Symptom experiences during chemotherapy treatment—With focus on nausea and vomiting," *European Journal of Oncology Nursing*, vol. 10, pp. 21–29, 2 2006.
- [117] R. L. Massey, H. K. Kim, and S. Abdi, "Brief review: Chemotherapy-induced painful peripheral neuropathy (CIPPN): Current status and future directions," *Canadian Journal of Anesthesia*, vol. 61, pp. 754–762, 5 2014.
- [118] T. Lammers, F. Kiessling, W. E. Hennink, and G. Storm, "Drug targeting to tumors: Principles, pitfalls and (pre-) clinical progress," *Journal of Controlled Release*, vol. 161, pp. 175–187, 7 2012.
- [119] K. D. Evans and A. McClure, "Using High-Intensity Focused Ultrasound as a Means to Provide Targeted Drug Delivery," *Journal of Diagnostic Medical Sonography*, vol. 32, no. 6, pp. 343–350, 2016.
- [120] F. Barreras, H. Amaveda, and A. Lozano, "Transient high-frequency ultrasonic water atomization," *Experiments in Fluids*, vol. 33, no. 3, pp. 405–413, 2002.
- [121] A. J. James, B. Vukasinovic, M. K. Smith, and A. Glezer, "Vibration-induced drop atomization and bursting," *Journal of Fluid Mechanics*, vol. 476, pp. 1–28, 2 2003.
- [122] S. Ueha, E. Mori, and N. Maehara, "Mechanism of ultrasonic atomization using a multipinhole plate," *Journal of the Acoustical Society of Japan (E)*, vol. 6, no. 1, pp. 21–26, 1985.
- [123] J. Kreula, P. Virkkunen, and S. Bondestam, "Effect of suction on specimen size in fine-needle aspiration biopsy," *Investigative Radiology*, vol. 25, no. 11, pp. 1175–1181, 1990.
- [124] L. Mancía, E. Vlasisavljevich, Z. Xu, and E. Johnsen, "Predicting Tissue Susceptibility to Mechanical Cavitation Damage in Therapeutic Ultrasound," *Ultrasound in Medicine and Biology*, vol. 43, no. 7, pp. 1421–1440, 2017.
- [125] E. Vlasisavljevich, J. Greve, X. Cheng, K. Ives, J. Shi, L. Jin, A. Arvidson, T. Hall, T. H. Welling, G. Owens, W. Roberts, and Z. Xu, "Non-Invasive Ultrasound Liver Ablation Using Histotripsy: Chronic Study in an In Vivo Rodent Model," *Ultrasound in Medicine and Biology*, vol. 42, pp. 1890–1902, 8 2016.
- [126] J. Chen, L. B. Priddy, R. Prabhu, E. Marin, L. Williams, M. Horstemeyer, and J. Liao, "Traumatic injury: Mechanical response of porcine liver tissue under high strain rate compression testing," in *Proceedings of the ASME Summer Bioengineering Conference 2009, SBC2009*, no. PART A, pp. 601–602, 2009.





ISBN 978-952-64-0933-7 (printed)  
ISBN 978-952-64-0934-4 (pdf)  
ISSN 1799-4934 (printed)  
ISSN 1799-4942 (pdf)

**Aalto University**  
**School of Science**  
**Department of Neuroscience and Biomedical Engineering**  
[www.aalto.fi](http://www.aalto.fi)

**BUSINESS +  
ECONOMY**

**ART +  
DESIGN +  
ARCHITECTURE**

**SCIENCE +  
TECHNOLOGY**

**CROSSOVER**

**DOCTORAL  
THESES**